Abrupt intrinsic and extrinsic responses of southwestern Iberian vegetation to millennial-scale variability over the past 28 ka

ANNA CUTMORE,[1,2]* BLANCA AUSÍN,[3,4] MARK MASLIN,[1] TIMOTHY EGLINTON,[4] DAVID HODELL,[5] FRANCESCO MUSCHITIELLO,[6,7] LAURIE MENVIEL,[8] NEGAR HAGHIPOUR,[4,9] BELEN MARTRAT,[10] VASILIKI MARGARI[1] and POLYCHRONIS C. TZEDAKIS[1]

[1]Department of Geography, University College London, London, United Kingdom
[2]Department of Marine Microbiology and Biogeochemistry, NIOZ Royal Institute for Sea Research, Netherlands
[3]Geography Department, University of Salamanca, Salamanca, Spain
[4]Geological Institute, ETH Zürich, Zürich, Switzerland
[5]Department of Earth Sciences, University of Cambridge, Cambridge, United Kingdom
[6]Department of Geography, University of Cambridge, Cambridge, United Kingdom
[7]NORCE Norwegian Research Centre, Bergen, Norway
[8]Climate Change Research Centre, University of New South Wales, Sydney, Australia
[9]Laboratory for Ion Beam Physics, ETH Zürich, Zürich, Switzerland
[10]Department of Environmental Chemistry, Spanish Council for Scientific Research (CSIC), Institute of Environmental Assessment and Water Research (IDAEA), Barcelona, Spain

ABSTRACT: We present new high-resolution pollen records combined with palaeoceanographic proxies from the same samples in deep-sea cores SHAK06-5K and MD01-2444 on the southwestern Iberian Margin, documenting regional vegetation responses to orbital and millennial-scale climate changes over the last 28 ka. The chronology of these records is based on high-resolution radiocarbon dates of monospecific samples of the planktonic foraminifera *Globigerina bulloides*, measured from SHAK06-5K and MD01-2444 and aligned using an automated stratigraphical alignment method. Changes in temperate and steppe vegetation during Marine Isotope Stage 2 are closely coupled with sea surface temperature (SST) and global ice-volume changes. The peak expansion of thermophilous woodland between ~10.1 and 8.4 cal ka BP lags behind the boreal summer insolation maximum by ~2 ka, possibly arising from residual high-latitude ice-sheets into the Holocene. Rapid changes in pollen percentages are coeval with abrupt transitions in SSTs, precipitation and winter temperature at the onset and end of Heinrich Stadial 2, the ice-rafted debris event and end of Heinrich Stadial 1, and the onset of the Younger Dryas, suggesting extrinsically forced southwestern Iberian ecosystem changes by abrupt North Atlantic climate events. In contrast, the abrupt decline in thermophilous elements at ~7.8 cal ka BP indicates an intrinsically mediated abrupt vegetation response to the gradually declining boreal insolation, potentially resulting from the crossing of a seasonality of precipitation threshold. © 2021 The Authors. *Journal of Quaternary Science* Published by John Wiley & Sons, Ltd.

KEYWORDS: abrupt climate change; Holocene; Marine Isotope Stage 2; pollen; southwest Iberia

Introduction

Situated in a transition zone between temperate central Europe and arid North Africa, the western Mediterranean is heavily affected by mid-latitude and sub-tropical interactions, making it sensitive to variations in the general circulation (Giorgi and Lionello, 2008; Lionello, 2012). With projections of increasingly severe and regular heatwaves and droughts (e.g. Lionello *et al.*, 2014 and references therein), greater understanding of the mechanisms by which temperature, water availability and consequently, vegetation, in this region respond to changing background conditions is urgently required.

The southwestern (SW) Iberian Margin has emerged as one of the most important locations for investigating orbital- and millennial-scale changes in the coupled ocean–land system, where analyses of palaeoceanographic and terrestrial proxies

from the same samples in marine sequences allow an *in situ* assessment of the relative timing of changes (e.g. Shackleton *et al.*, 2000, 2003; Sánchez Goñi *et al.*, 2000; Tzedakis *et al.*, 2004, 2018; Margari *et al.*, 2010, 2020). This is a direct consequence of the geographic setting of the area, where the combined effects of major river systems and a narrow continental shelf with a steep slope into the abyssal plain lead to rapid transport of terrestrial material to deep-water environments (Vanney and Mougenot, 1981; Naughton *et al.*, 2007). This results in high accumulation rates and enables a direct comparison with co-occurring marine proxies (Hodell *et al.*, 2013a).

Marine Isotope Stage (MIS) 2 26–11.7 ka) and the Holocene interglacial (11.7 ka – present) encompass several abrupt climate events in the North Atlantic superimposed on orbital-scale global changes that include the expansion of Northern Hemisphere ice sheets, deglaciation, and the establishment of interglacial conditions (Dansgaard *et al.*, 1982, 1993; Broecker *et al.*, 1992; Bond *et al.*, 1992; NGRIP

*Correspondence: A. Cutmore, as above.
E-mail: anna.cutmore.15@ucl.ac.uk

Members, 2004). This period includes the abrupt cold events of Heinrich Stadial 2 (HS2; 24.3–23.3 ka; Barker *et al.*, 2009) and Heinrich Stadial 1 (HS1)/Mystery Interval (17.5–14.5 ka; Denton *et al.*, 2006) which bracketed the Last Glacial Maximum (LGM) (22–19 ka; Yokoyama *et al.*, 2000), the abrupt warming at the onset of the Bølling–Allerød (BA) interstadial (14.7–12.9 ka; Hartz and Milthers, 1901; Magny *et al.*, 2003a; Rasmussen *et al.*, 2006), the Younger Dryas (YD) event (12.9–11.7; Watts, 1977, 1980; Mott *et al.*, 1986; Magny *et al.*, 2003a; Rasmussen *et al.*, 2006), and the 8.2 ka event (Alley *et al.*, 1997; Bond *et al.*, 1997; Magny *et al.*, 2003b). Consequently, the last 28 ka can provide insight into the response of SW Iberian vegetation to external forcings on a variety of timescales and shed light on extrinsic and intrinsic abrupt SW Iberian vegetation changes in response to changing background conditions. An 'extrinsic' abrupt vegetation change is defined as a direct ecological response to an abrupt climate forcing, while an 'intrinsic' abrupt vegetation change is the result of a threshold/tipping point/non-linear feedback caused by a gradual climate forcing (Williams *et al.*, 2011).

Improving knowledge of ecological responses to both orbital and millennial-scale climate change is important for understanding the sensitivity of SW Iberian ecosystems, the different responses of taxa, and the implications of these changes on regional and global feedbacks. Here, we present two new high-resolution pollen records of the last 28 ka combined with palaeoceanographic analyses and a radiocarbon (^{14}C) chronology supported by 47 ^{14}C dates from deep-sea cores SHAK06-5K and MD01-2444 on the SW Iberian Margin, to:

1. investigate the response of SW Iberian vegetation to orbital variability over MIS 2 and the Holocene;
2. investigate the absolute timing of millennial-scale SW Iberian vegetation changes over the past 28 ka, and the relative timing of abrupt vegetation and oceanographic changes over this period using existing palaeoceanographic analyses from cores SHAK06-5K and MD01-2444; and
3. identify the presence of extrinsic and/or intrinsic ecological changes over the past 28 ka.

Environmental setting

Climate and vegetation of the study area

Western Iberia has an oceanic climate. The Tagus and Sado basins in SW Iberia are characterised by the high seasonality of the Mediterranean climate, with warm, dry summers and mild winters, where mean annual precipitation is <600 mm, the mean winter temperature is ~10°C and mean summer temperature is ~23°C (Fick and Hijmans, 2017). Although this region's dominant winds are northerly and westerly (Hurrell, 1995), occasional southerly winds can transport Saharan dust to SW Iberia (Rodríguez *et al.*, 2001).

In the present-day Tagus and Sado basins, coastal regions are dominated by thermophilous woodland, Mediterranean pines and maquis shrubs, which includes *Pinus pinaster* Aiton, *P. pinea, Quercus suber, Q. coccifera, Pistacia lentiscus, Phillyrea latifolia, Arbutus unedo, Olea europaea, Ceratonia siliqua* and *Erica arborea* (Morales-Molino *et al.*, 2020). The vegetation of the western and central Tagus basin and the inner Sado basin is primarily composed of scrub, orchards, vineyards and woodland. The latter is dominated by *Q. ilex* subsp. *rotundifolia* and *Q. suber* forests with a considerable presence of Mediterranean pines and deciduous oaks, as well as other Mediterranean elements including *Phillyrea angustifolia* and *Pistacia terebinthus* (Blanco Castro *et al.*, 1997;

Morales-Molino *et al.*, 2020). At mid-elevation (700–1000 m above sea level (a.s.l.)), forests are dominated by deciduous *Quercus* species, including *Q. pyrenaica* and *Q. faginea*, along with sub-Mediterranean and Eurosiberian elements, *Pinus sylvestris, P. nigra, Juniperus thurifera* and *Taxus baccata* (Blanco Castro *et al.*, 1997; Morales-Molino *et al.*, 2020). Where degradation of this woodland occurs, two types of matorral communities can form: Cistaceae scrubland in regions with an annual rainfall between 600 and 1000 mm, and Ericaceae communities where precipitation is higher (Blanco Castro *et al.*, 1997). In the highest elevation regions of the central and eastern Tagus basin, *P. nigra* and *P. sylvestris* forests dominate, with deciduous *Q. pyrenaica* woodland also present. In areas where human interference has reduced soil cover, matorral scrub occurs which includes Cistaceae, *Erica, Calluna*, Genisteae and Lamiaceae (Polunin and Smithies, 1973; Blanco Castro *et al.*, 1997; Morales-Molino *et al.*, 2020). Although greatly disturbed by anthropogenic activity, particularly olive groves and vineyards on the fertile river soils (Aguiar and Ferreira, 2005), riparian woodland in the Tagus basin is dominated by *Fraxinus angustifolia, Alnus glutinosa, Populus nigra, Salix alba* and *S. salviifolia*, with the edge of these forest environments often surrounded by *Rubus ulmifolius, Crataegus monogyna* and *Erica arborea* (Aguiar *et al.*, 2000). The Sado basin is predominately woodland and scrub, with large *Q. suber* forests in the south, although a substantial proportion of the land is used for arable purposes (Polunin and Smithies, 1973). Today, land use across Iberia is highly varied, influenced heavily by geological, climatic and anthropogenic conditions (Polunin and Smithies, 1973; Morales-Molino *et al.*, 2020). Much of the landscape is dedicated to farming, including a multifunctional agro-sylviopastoral system known as a 'Montado' in Portugal which eliminates shrubs in favour of evergreen and semi-evergreen *Quercus* spp. (primarily *Q. ilex* subsp. *rotundifolia* or *Q. suber*) and grasses.

Oceanographic setting

The Portugal Current (PC) is the dominant surface current (Fig. 1), transporting cold surface waters equatorward (Pérez *et al.*, 2001). Between June and September this is enhanced with the strengthening of the Azores anticyclonic cell and weakening of the Icelandic low, intensifying northerly and northwesterly winds along the Portuguese coast (Fiúza *et al.*, 1982; Relvas *et al.*, 2007). This drives strong upwelling of cold nutrient-rich waters from 60–120 m water depth and promotes primary productivity (Abrantes, 1992), while low energy waves lead to upper-level stratification (Jorge da Silva, 1992). Between October and March, the strengthened Icelandic low and weakened Azores High result in southward-shifted westerlies; these dominant and strong southwesterly winds create down-welling over the Iberian Margin continental shelf (Ambar andand Fiúza, 1994; Vitorino *et al.*, 2002), and drive the poleward Portugal Coastal Counter current (PCCC). This winter cooling of surface waters combined with high energy waves creates well mixed surface waters to ~100 m (Vitorino *et al.*, 2002). These surface currents are therefore directly linked to atmospheric circulation and are sensitive to rapid atmospheric changes.

At mid-depth (500–1700 m), the Iberian Margin is dominated by northward-flowing, warm, salty Mediterranean overflow water, formed by the mixing of Mediterranean Sea and Atlantic Ocean water in the Gulf of Cadiz (van Aken, 2000a). Under this, at ~1600 m, flows Labrador Sea Water – the upper component of North Atlantic deep water (NADW), which is underlain by northeastern Atlantic deep water and lower deep water (derived from Antarctic bottom water) (van Aken, 2000b;
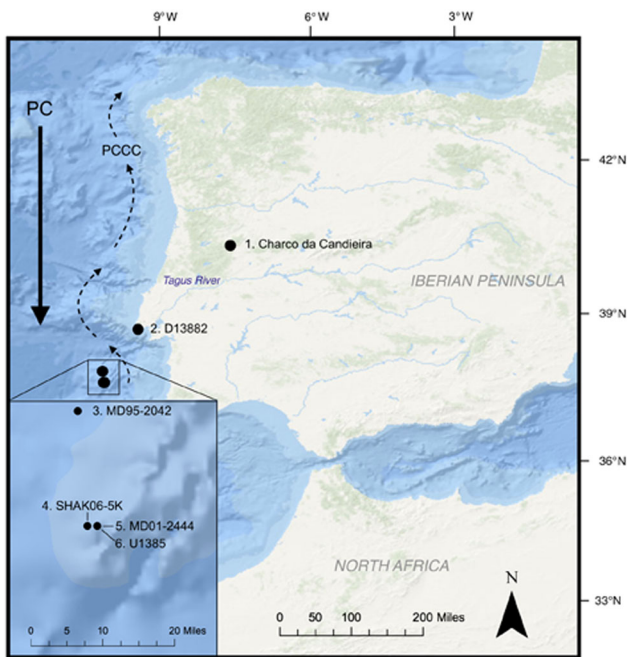
Figure 1. Sites of southwestern Iberian pollen records mentioned in this study: 1. Charco da Candieira (Van der Knaap and van Leeuwen, 1997); 2. D13882 (Gomes *et al.*, 2020); 3. MD95-2042 (Chabaud *et al.*, 2014); 4. SHAK06-5K (this study); 5. MD01-2444 (this study); 6. U1385 (Oliveira *et al.*, 2018). PC: Portugal Current; PCCC: Portugal Coastal Counter Current. [Color figure can be viewed at wileyonlinelibrary.com]

Voelker and de Abreu, 2011). Today, deep water is dominated by NADW components with Antarctic-originating lower deep water below 4000 m, although during the Last Glacial, the contribution of southern-sourced water was more significant (Skinner *et al.*, 2003; Martrat *et al.*, 2007).

Sediment supply to the SW Iberian Margin

The dominant sediment supply to the SW Iberian Margin is from the Tagus River, followed by the Sado River (Jouanneau *et al.*, 1998). The former has a catchment area of 80 600 km^2 and is 1110 km in length (Vale, 1990), while the latter has a catchment area of 7640 km^2 and is 175 km in length (Loureiro *et al.*, 1986). Although the annual suspended sediment load is 0.4–1 $\times 10^6$ t for the Tagus River and ~15 $\times 10^3$ t for the Sado River, most sediment discharge occurs during the winter months when river flow is highest (Vale and Sundby, 1987; Vale *et al.*, 1993). Short-distance wind transport transfers pollen into these rivers, directly from the plants and topsoil, but as the Iberian Margin's dominant wind source is northerly and westerly over the Atlantic (Hurrell, 1995), significant aeolian transport of pollen from the continent to the marine environment is likely to be limited (Sánchez Goñi *et al.*, 1999; Naughton *et al.*, 2007), meaning that the dominant pollen transport mechanism to our core site is likely to be fluvial.

The SW Iberian continental shelf is narrow, on average 20–30 km wide, dissected by several submarine canyons, notably the Cascais and Lisbon–Sebútal canyons (Arzola *et al.*, 2008) (Fig. S1). Sediment reaching the outer shelf can be transported onto the continental slope or deep ocean via the Cascais and Lisbon–Sebútal canyons, acting as the primary sinks for terrestrial material into the Tagus Abyssal Plain (de Stigter *et al.*, 2011). Although the source of terrestrial sediment transported to the SW Iberian Margin has remained constant over the last 28 ka, primarily supplied by the Tagus catchment basin (with a small contribution from the Sado

catchment basin), the depocentre of this terrestrial material changed over the last deglaciation (Jouanneau *et al.*, 1998). During MIS 2, the sediment supply to the Tagus Abyssal Plain was significantly higher than in the Holocene, influenced by the lowered sea levels of this period which directly and rapidly transported material via the Cascais and Sebútal–Lisbon canyons into the deep sea (Vis *et al.*, 2008, 2016; Lebreiro *et al.*, 2009; de Stigter *et al.*, 2011). Today, the higher sea levels and flooding of the continental shelf have disconnected the canyons from the Tagus's sediment supply, moving the depocentre landwards and reducing deep-ocean sediment deposition (Vis *et al.*, 2008, 2016; Vis and Kasse, 2009).

Materials and methods

During the 2013 *James Cook* cruise, kasten core SHAK06-5K (3.44 m length) was recovered from 2646 m depth on the SW Iberian Margin (37°34 N, 10°09 W) (Hodell *et al.*, 2014). The site is located on the Promontório do Príncipe de Avis spur (Fig. S1), ~115 km east of the Portuguese coast and southwest of the Tagus and Sado rivers. Calypso piston core MD01-2444 (27.5 m length) was retrieved from the same area (37°34 N, 10°09 W) at a depth of 2637 m during the 2001 R/V *Marion Dufresne II* Geosciences Cruise (Vautravers and Shackleton, 2006; Hodell *et al.*, 2013a).

Pollen analysis

SHAK06-5K samples were taken at 2 cm intervals ($n = 165$; 0–329 cm), increasing to every 1 cm between 46 and 64 cm due to this section's reduced sediment accumulation rate (SAR). MD01-2444 samples were taken at ~3 cm intervals ($n = 42$; 121–238 cm). Some 6–7 g of dry marine sediment was used, adding *Lycopodium* tablets of a known quantity to quantify the absolute pollen concentration (Stockmarr, 1971). The UCL Department of Geography Marine Fossil Pollen Preparation Method (Margari, 2016) was followed to extract the pollen. This eluted calcium carbonate, humic acids, organic material, silicates, and sulphides and pyrites from the sediment, using 10% HCl, 10% KOH, a 180 µm sieve, 40% HF and 10% HNO_3, respectively. Safranin was added to stain the pollen residue, tertiary-butyl alcohol acted as a dehydrating agent, and silicone oil was added to suspend grains for turning (Matthews, 1969). Each sample was prepared on microscope slides and 100 grains (excluding *Pinus*, *Cedrus*, aquatics, pteridophytes, algae and indeterminate grains) were counted and identified for each sample using a compound microscope (×400 and ×1000 magnification). Pollen was identified to its lowest possible taxonomic levels using the pollen identification manual for European and Middle Eastern flora (Reille, 1999; Beug, 2004), with nomenclature following *Mabberley's Plant-book* (Mabberley, 2017).

The total pollen sum represents all grains encountered in each sample excluding indeterminate grains, *Pinus* (owing to its overrepresentation in marine samples; Hopkins, 1950), and aquatics, pteridophytes and algae (in order to focus on broad regional changes). *Cedrus* was also removed from the total sum due to its significant presence in North Africa over the Last Glacial period and Holocene, meaning it likely reflects long-distance transport (Lamb and van der Kaars, 1995; Magri and Parra, 2002; Bell and Fletcher, 2016). Pollen concentration (grains g^{-1}) was quantified using the pollen and *Lycopodium* count, total *Lycopodium* spores per tablet, and the sediment quantity (g) (Stockmarr, 1971). Several isolated extreme pollen concentration values ($n = 3$; 96, 168 and 314 cm) were removed from the diagrams so as not to distort the summary

curves and to facilitate the assessment of the overall pollen concentration pattern. The pollen accumulation rate (PAR; grains cm^{-2} ka^{-1}) was calculated using pollen concentration, the SAR, and the dry bulk density of the sediment.

Pollen diagrams

Pollen zonation diagrams were constructed with PSMIPOLL software (Bennett, 2011) using 'optimal splitting using information content' to create the pollen assemblage zones (PAZs), including taxa ≥1% in the zonation. The positioning and number of zones were manually reviewed and edited, with 12 PAZs constructed for the SHAK06-5K record (assigned the prefix 'SHAK06-') and eight PAZs constructed for the MD01-2444 record (assigned the prefix 'MD01-'). Pollen diagrams are plotted as a function of depth, presenting all taxa in pollen percentages (%), calculated using the main pollen sum and taxon count.

Arboreal pollen includes all trees and shrubs minus *Pinus* and *Cedrus*. Pioneer species include *Betula*, *Hippophae*, *Juniperus* and *Salix*, while Mediterranean taxa include *Phillyrea*, *Pistacia*, *Olea* and evergreen *Quercus*. Eurosiberian species represent all arboreal pollen excluding pioneer and Mediterranean taxa, while Mediterranean and Eurosiberian percentages are combined as 'temperate arboreal taxa', with these combined elements representing thermophilous woodland. Herbaceous taxa (non-arboreal pollen) are divided into steppe (Amaranthaceae, *Artemisia*, Poaceae and *Ephedra*), and ubiquitous herbs.

Chronological framework

Accelerator mass spectrometry (AMS) ^{14}C ages of monospecific samples of the planktonic foraminifera *G. bulloides* were measured from cores SHAK06-5K ($n = 40$) and MD01-2444 ($n = 7$) to create a master chronology on the SHAK06-5K depth scale. While the 40 AMS ^{14}C measurements from core SHAK06-5K have previously been published in Ausín et al. (2019a), new AMS ^{14}C dates were measured from core MD01-2444. Isolation of *G. bulloides* specimens from MD01-2444 samples took place at UCL's Department of Geography with ~15 g of wet sediment taken from 10 regularly spaced depths, diluted with deionised water and disaggregated using a centrifuge tube rotator for ~2 hours. Samples were wet-sieved (300–250 μm), washed using a high-pressure deionised water stream, and oven-dried (~10 h; 60°C). From this fraction ~200 well-preserved *G. bulloides* specimens were picked.

AMS ^{14}C measurements (^{14}C/^{12}C) were determined at ETH Zürich's Laboratory of Ion Beam Physics using a Mini Carbon Dating System (MICADAS) with a gaseous ion source (Synal et al., 2007) following the method outlined by Wacker et al. (2013) and Ausín et al. (2019a). Surface contaminants were leached (referred to, hereafter, as the leachate) from the foraminifera and the CO_2 of the leachate measured for [14]C. The leachate displays younger values than the main fraction in all but two samples (121 and 151 cm; Table S1), demonstrating successful surface contaminant removal of secondary calcite or exogenous carbon (Wacker et al., 2013; Bard et al., 2015; Ausín et al., 2019a). In sample 121 cm of core MD01-2444, the difference between the values of the leachate and main fraction is within the margin of error (±1σ), while that of 151 cm is not (consequently, this sample was excluded from the age model). The CO_2 of the remaining sample (referred to as the main fraction) was measured for ^{14}C on two gas targets.

International Atomic Energy Agency reference materials C1 and C2 were used; the former as a blank and the latter as an internal standard. For fractionation correction and normalisation, oxalic acid II NIST SRM 4990 standard was used. The measured ^{14}C/^{12}C ratios are corrected and reported as fraction modern (F[14]C) according to Stuiver and Polach (1977) and Reimer et al. (2004). The measurement precision is better than 5‰ for modern samples, with the data processing conducted using BATs Software (Wacker et al., 2010).

The stratigraphical alignment of the cores was modelled using an automated algorithm based on Bayesian Markov-chain Monte Carlo (MCMC) inversion. The approach builds on previous work presented in Muschitiello et al. (2020) and has been successfully applied on a variety of palaeoceanographic records (Muschitiello et al., 2019; Sessford et al., 2019; West et al., 2019). A robust multi-parameter alignment was performed that simultaneously correlates the input and target stratigraphies using two independent proxy signals. We used the X-ray fluorescence (XRF) Ca/Ti and ^{14}C records from core MD01-2444 as inputs (Hodell et al., 2013a) and their counterpart records from core SHAK06-5K as targets (Ausín et al., 2020) (Fig. S2). The algorithm was run for 10^6 iterations after discarding the initial 10^5 MCMC samples ('burn-in'). The median of the MCMC alignment sample was used to infer the posterior optimal correlation between MD01-2444 and SHAK06-5K, while its variability was used to estimate the posterior uncertainty of the overall alignment. The algorithm hinges on the assumption of direct synchrony of fluctuations in the Ca/Ti signals and *G. bulloides* AMS ^{14}C ages at both coring sites and circumvents the limitations associated with subjective and point-wise visual alignments, thus providing a reproducible and continuous alignment that accounts for potential uneven compaction/expansion in the sediment cores. The alignment served to transfer the MD01-2444 dates onto the SHAK06-5K stratigraphy in order to create a combined 'master' Bayesian age model.

In SHAK06-5K, planktic foraminiferal ^{14}C ages continuously increase downcore and all 40 samples are used in the age model. While this is predominately the case in MD01-2444, one ^{14}C age was rejected (151 cm) as it reflects older material and the MCMC stratigraphical alignment also highlighted two further ^{14}C age reversals (232 and 238 cm; Fig. S3), which were removed from the age model.

Seven new MD01-2444 ^{14}C dates transferred onto the SHAK06-5K stratigraphy and 40 ^{14}C dates from SHAK06-5K were used in the production of the master age model. A Bayesian depositional age–depth model (*P_sequence*) was created using the calibration package Oxcal 4.4 (Bronk Ramsey, 2009), and the Marine20 calibration curve (Heaton et al., 2020), which applies a temporally variable reservoir (R) age beyond the Holocene. There is still an apparent offset of the cold-to-warm and warm-to-cold transitions in our record compared with those published in the literature. Using our age model, the onset of the Holocene is dated at 12 ka ± 525 yrs, the start of the YD is 13.2 ka ± 350 yrs, the BA begins at 15.4 ka ± 375 yrs, HS1 and HS2 start at 18.2 ka ± 400 yrs and 25.7 ka ± 410 yrs, respectively, while the LGM begins at 23.6 ka ± 320 yrs. This offset is likely to be affected in part by the estimated uncertainty of the Marine20 calibrated age model (Table 1; ±2σ) as well as the spatiotemporal variability in the Iberian Margin's R-age over the Last Glacial and subsequent deglaciation (Waelbroeck et al., 2001; Stern and Lisiecki, 2013; Freeman et al., 2016; Skinner et al., 2019). While the spatiotemporal variability of the Iberian Margin's R-age over this period is widely acknowledged, its quantification is still debated, with divergent estimates reaching differences of up to 550 years (Ausín et al., 2021; Skinner et al., 2021). Consequently, a local R-age has not been added to our calibration.

The master age model indicates that the SHAK06-5K pollen record spans the past 27.4 cal ka BP, while the pollen record of MD01-2444 covers 5.7–13.5 cal ka BP. The SAR of the master

Table 1.   The master age–depth model based on 40 published monospecific planktonic foraminifera *G. bulloides* samples from SHAK06-5K (Ausín *et al.*, 2019a) and seven new ^{14}C dates from MD01-2444 (shaded in grey). The alignment of the cores, transferring the MD01-2444 samples onto the SHAK06-5K depth scale, is produced by an automated proxy-to-proxy stratigraphical alignment algorithm. [14]C values and errors were not rounded during the method stage to prevent propagated errors and artificial offsets but have been rounded in this table to follow convention.

Core	Lab code	Master depth (cm)	Radiocarbon age ([14]C a BP)	± 1σ	Calendar age (cal a BP)	± 2σ
SHAK06-5K	82182.2.1	0	790	± 150	255	± 228
SHAK06-5K	82183.2.1	4	1010	± 150	433	± 210
SHAK06-5K	72979.2.1	10	1250	± 70	662	± 148
SHAK06-5K	82185.2.1	14	1450	± 70	834	± 165
SHAK06-5K	72981.2.1	20	1820	± 55	1202	± 159
SHAK06-5K	72983.2.1	30	2300	± 50	1749	± 181
SHAK06-5K	72985.2.1	40	3090	± 65	2731	± 217
SHAK06-5K	75040.1.1	44	3620	± 75	3334	± 208
SHAK06-5K	70397.1.1	48	3760	± 60	3542	± 193
SHAK06-5K	75041.1.1	54	5300	± 80	5514	± 202
MD01-2444	102679.1.1	55	5500	± 65	5655	± 195
MD01-2444	102678.1.1	59	7320	± 80	7649	± 170
SHAK06-5K	72987.2.1	60	7470	± 60	7714	± 151
MD01-2444	102676.1.1	64	7680	± 95	7990	± 231
MD01-2444	102675.1.1	66	8010	± 85	8306	± 244
MD01-2444	102674.1.1	67	8380	± 95	8741	± 303
MD01-2444	102673.1.1	69	8600	± 90	9108	± 229
SHAK06-5K	72989.2.1	70	8740	± 70	9175	± 197
MD01-2444	102672.1.1	72	9550	± 95	10 261	± 300
SHAK06-5K	75042.1.1	76	9960	± 80	10 821	± 283
SHAK06-5K	72991.2.1	82	11 050	± 85	12 336	± 287
SHAK06-5K	72993.2.1	90	11 450	± 90	12 795	± 201
SHAK06-5K	70400.1.1	100	12 100	± 110	13 404	± 248
SHAK06-5K	72995.2.1	110	12 400	± 100	13 848	± 276
SHAK06-5K	72997.2.1	120	13 250	± 95	15 050	± 309
SHAK06-5K	70403.1.1	130	13 600	± 110	15 581	± 313
SHAK06-5K	72999.2.1	140	14 100	± 100	16 209	± 285
SHAK06-5K	75043.1.1	146	14 300	± 100	16 527	± 295
SHAK06-5K	73001.2.1	152	14 900	± 100	17 063	± 256
SHAK06-5K	73002.2.1	160	14 900	± 110	17 291	± 269
SHAK06-5K	73003.2.1	172	15 350	± 110	17 839	± 306
SHAK06-5K	73005.2.1	180	15 950	± 140	18 394	± 304
SHAK06-5K	75044.1.1	196	16 650	± 120	19 274	± 303
SHAK06-5K	75016.1.1	200	17 100	± 120	19 596	± 285
SHAK06-5K	75018.1.1	210	17 300	± 120	19 964	± 281
SHAK06-5K	75020.1.1	220	17 400	± 140	20 298	± 321
SHAK06-5K	75022.1.1	230	18 600	± 180	21 381	± 420
SHAK06-5K	75024.1.1	240	18 750	± 140	21 839	± 352
SHAK06-5K	70406.1.1	260	20 000	± 180	23 098	± 373
SHAK06-5K	75028.1.1	270	20 400	± 150	23 556	± 304
SHAK06-5K	75030.1.1	280	20 700	± 150	23 988	± 284
SHAK06-5K	75048.1.1	284	21 000	± 160	24 229	± 332
SHAK06-5K	75032.1.1	290	21 300	± 160	24 621	± 376
SHAK06-5K	75033.1.1	300	22 100	± 170	25 432	± 339
SHAK06-5K	75034.1.1	310	22 600	± 180	25 965	± 318
SHAK06-5K	75036.1.1	320	23 000	± 180	26 506	± 407
SHAK06-5K	75038.1.1	329	24 100	± 200	27 395	± 358

sequence (Fig. 2) has been calculated using the Bayesian *P_sequence* model in Oxcal 4.4, which assumes random deposition (Bronk Ramsey, 2007).

Intrinsic/extrinsic vegetation response

To quantitatively analyse the response of SW Iberian vegetation to abrupt climate events over the past 28 ka, the rate of change (RoC) of the SHAK06-5K vegetation records was calculated and compared with the RoC of climate model and proxy climate records from this region. Temperate and steppe pollen records from SHAK06-5K were used to assess the vegetation RoC (Grimm and Jacobson, 1992), while simulated annual precipitation (cm yr^{-1}) and surface air temperature for December, January and February (DJF SAT) (°C) over Iberia, and $U^{K'}_{37}$–derived Iberian

Margin SSTs from MD01-2444 (Martrat *et al.*, 2007) were used as regional climate forcings. DJF SAT was used as winter temperatures as winter temperatures have an important influence on the functioning of temperate ecosystems (Kreyling, 2010). Western Iberian DJF SAT and annual precipitation (9–2°W, 39–43°N) were extracted from transient experiments of the Last Glacial period (here 29.9–18 cal ka BP, Menviel *et al.*, 2014), deglaciation and Holocene (18–2 cal ka BP, Menviel *et al.*, 2011), performed with the Earth system model of intermediate complexity, LOVECLIM (Goosse *et al.*, 2010). The experiments were forced with time varying changes in orbital parameters (Berger, 1978), Northern Hemispheric ice-sheet topography, extent, and albedo (Abe-Ouchi *et al.*, 2007), and atmospheric CO_2 concentration (Ahn and Brook, 2014). To mimic millennial-scale climate variability associated with Heinrich events and the YD, meltwater is added into the North Atlantic, thus

leading to Atlantic Meridional Overturning Circulation (AMOC) variations.

Gaussian interpolation was used to smooth and resample the simulated climate records and the SST and pollen time series every 200 years, although for the vegetation and SST records, gaps in Gaussian interpolations were filled with linear interpolation over intervals of particularly low sampling resolution (~50–83 cm). The RoC was calculated for the simulated and proxy climate records by taking the difference between consecutive samples every 200 years, then normalising the data by subtracting the mean and dividing by the standard deviation, and transforming all values into positives. To define an abrupt event, the RoC in the model and proxy records had to meet the criterion of a minimum of two data points in succession that exceeded 1σ. One exception to this rule is the abrupt DJF SAT increase at the end of HS2, where one value falls slightly below 1σ (0.87). The RoCs of its neighbouring samples, however, exceed the 1σ threshold as does the mean RoC of the three samples together; consequently, the rapid SAT increase at the end of HS2 was accepted as an abrupt event. As the timings of these abrupt changes in the simulated and proxy records do not always have the same age, only the RoC of abrupt climate transitions are analysed and compared.
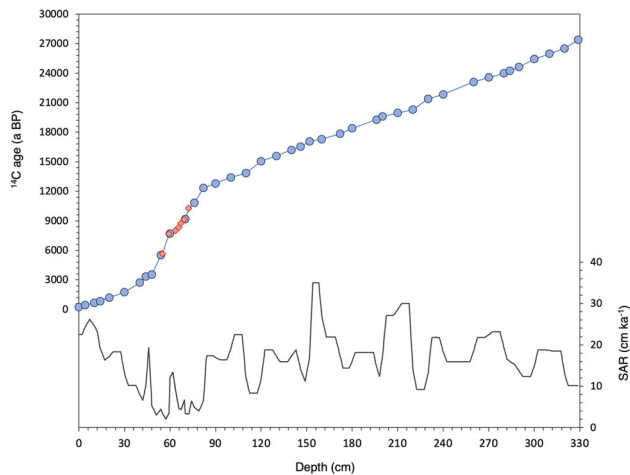
Results and discussion

Features of the whole sequences

A range of pollen and spores were identified in SHAK06-5K and MD01-2444, which include angiosperms, gymnosperms, pteridophytes and bryophytes. Of the taxa included in the pollen sums, 69 different taxa were identified in the SHAK06-5K record: 25 trees and shrubs and 44 herbaceous taxa. In MD01-2444, 52 different taxa were identified: 19 trees and shrubs, and 33 herbaceous taxa. Although 42 samples were prepared from MD01-2444, five were devoid of pollen (127, 130, 136, 139 and 142 cm). Both cores have good pollen preservation, with the percentage of indeterminate grains being 4 and 16%, respectively. The main features of the pollen records are illustrated in Figs. 3 and 4, while the dominant vegetation of each PAZ is outlined in Tables 2 and 3.
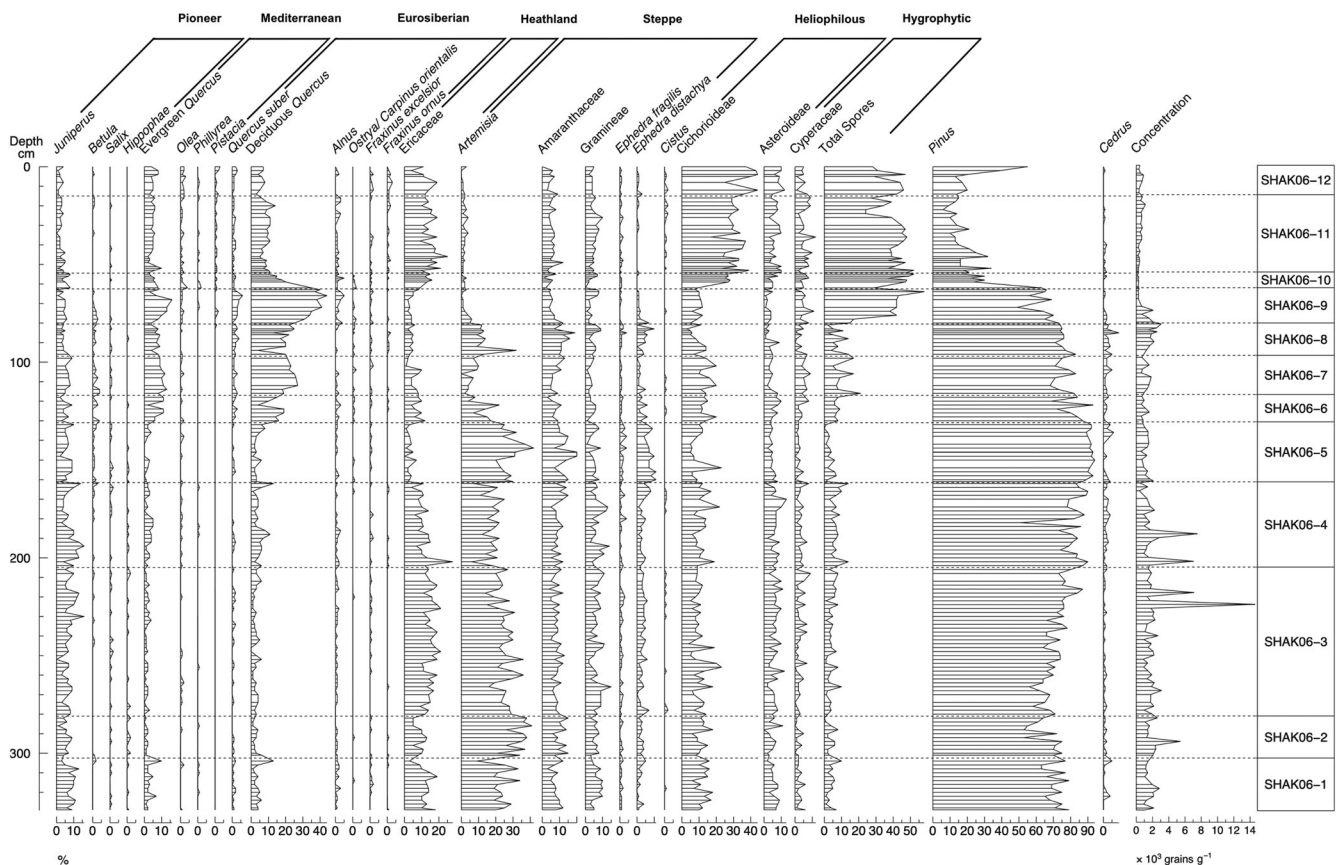
Figure 2. Master calibrated age–depth model (cal a BP), created using 40 AMS ^{14}C dates from SHAK06-5K (blue dots) and seven from MD01-2444 (red diamonds). Black line shows sediment accumulation rate (SAR; cm ka^{-1}). Both the age–depth model and SAR produced using a *P_sequence* depositional model in OxCal. [Color figure can be viewed at wileyonlinelibrary.com]

Figure 3. SHAK06-5K pollen diagram showing change in pollen percentages (%) with depth (cm) and changes in the total pollen concentration (×10^3 grains g^{-1}). The main vegetation features of the pollen assemblage zones are described in Table 2. Total spores includes *Isoetes*.
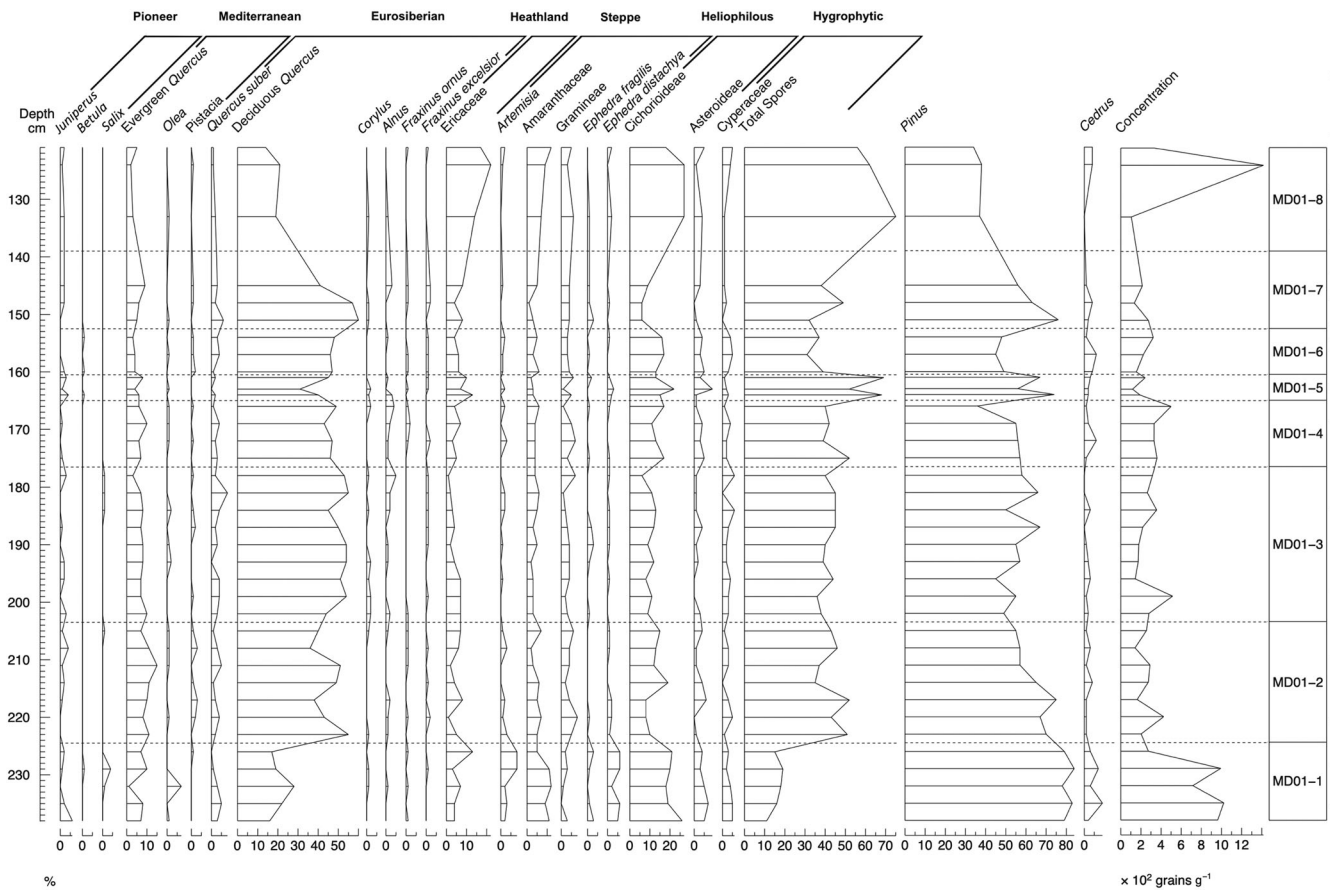
Figure 4. MD01-2444 pollen diagram showing changes in pollen percentages (%) with depth (cm) and changes in the total pollen concentration ($\times 10^2$ grains g^{-1}). The main vegetation features of the pollen assemblage zones are described in Table 3. Total spores includes *Isoetes*.

Table 2. The main vegetation features of each pollen assemblage zone in core SHAK06-5K.

Zone	Depth (cm)	Vegetation	Main pollen signature
SHAK06 – 1	329 – 302.5	Steppe	Steppe taxa dominate (~40%), primarily composed of *Artemisia* (~23%).
SHAK06 – 2	302.5 – 281	Semi-desert/steppe	Rise in semi-desert taxa (*Artemisia* and Amaranthaceae) (reaching 52%), dominated by *Artemisia* (~33%).
SHAK06 – 3	281 – 205	Steppe	Reduced semi-desert taxa (~33%), primarily Artemisia (~25%) and increase in Ericaceae (~15%).
SHAK06 – 4	205 – 161.5	Steppe/open mixed woodland	Rise in temperate taxa (reaching 22% at 188 cm), primarily composed of deciduous *Quercus*, followed by a decline (reaching 5% at 170 cm). High steppe taxa values (~40%).
SHAK06 – 5	161.5 – 131	Semi-desert/steppe	Steppe taxa rise to highest values of the record (reaching 68%), primarily composed of *Artemisia* (reaching 42%).
SHAK06 – 6	131 – 117	Steppe/open mixed woodland	Early rise in temperate taxa (26–37%) to 124 cm, with deciduous *Quercus* (16% to 19%) and evergreen *Quercus* (6% to 11%) contributing most significantly. Decline in deciduous *Quercus* at 122 cm (to 10%), recovering towards the upper boundary.
SHAK06 – 7	117 – 97	Mixed woodland	Increased temperate taxa (peaking at 47%), primarily made up of deciduous *Quercus* (~22%) with a rise in Mediterranean elements (~11%).
SHAK06 – 8	97 – 80.5	Steppe/open mixed woodland	Prominent rise in steppe taxa (~36%), primarily *Artemisia* and Amaranthaceae (~14% and ~12%, respectively) and reduced temperate taxa percentages (~30%).
SHAK06 – 9	80.5 – 62.5	Mixed forest	Increase in temperate taxa to highest percentages of the record (reaching 64%); predominately deciduous *Quercus* (~36%) and evergreen *Quercus* (~9%).
SHAK06 – 10	62.5 – 54.5	Open mixed woodland	Transitional zone of increased Ericaceae (~13%), reducing temperate taxa (~33%) and significant increase in Cichorioideae (~24%).
SHAK06 – 11	54.5 – 15	Open mixed woodland	Highest Ericaceae values of the record (reaching 25%), high Cichorioideae (~30%) and temperate taxa, dominated by deciduous *Quercus* (~9%) and evergreen *Quercus* (~5%).
SHAK06 – 12	15 – 0	Open mixed woodland	Highest percentages of Cichorioideae of the record (reaching 44%), increasing temperate taxa (12% to 19%) and initial rise, then decline (19% to 4%) in Ericaceae.

Table 3.　The main vegetation features of each pollen assemblage zone in core MD01-2444.

Zone	Depth (cm)	Vegetation	Main pollen signature
MD01 – 1	238 – 224.5	Open mixed woodland	Dominance of herbaceous taxa, particularly Cichorioideae (~20%) and steppe taxa (~21%), particularly Amaranthaceae (~9%), with presence of temperate taxa (~33%).
MD01 – 2	224.5 – 203.5	Mixed forest	Rise in temperate taxa (~62%), primarily deciduous *Quercus* (~44%) and Mediterranean elements evergreen *Quercus* (~10%) and Pistacia (~1%).
MD01 – 3	203.5 – 176.5	Mixed forest	Decline in evergreen *Quercus* (~7%), but rise in deciduous *Quercus* (~50%).
MD01 – 4	176.5 – 165	Mixed forest	Slight decline in temperate taxa (~61%), primarily due to a decline in deciduous *Quercus* (~45%).
MD01 – 5	165.5 – 160.5	Mixed forest	Overall decline in temperate taxa (~50%) due to significant reduction in deciduous *Quercus* (~38%) and rise in Ericaceae (~10%) and some herbaceous elements including Cichorioideae and Asteroideae.
MD01 – 6	160.5 – 152.5	Mixed forest	Overall increase but steady temperate percentages (~57%), dominated by deciduous *Quercus* (~45%).
MD01 – 7	152.5 – 139	Mixed forest	Rise in temperate taxa (~68%) dominated by Eurosiberian elements (reaching 68%), followed by a later rise in Mediterranean taxa (~10%) and rising Ericaceae percentages (~7%).
MD01 – 8	139 – 121	Open mixed woodland	Decline in temperate taxa (~25%) primarily deciduous *Quercus* (~17%) and rise in Ericaceae, reaching 21%, the highest of the record, and a rise in Cichorioideae, reaching 27%.

Variation in the deposition of terrestrially sourced material

The pollen concentration and PAR of SHAK06-5K is highest in the lower part of the core (MIS 2) (Fig. 5(d)–(e)). Between ~12 and 11 cal ka BP, PAR declines from 38 150 to 1990 grains cm^{-2} ka^{-1}, while the pollen concentration declines from 3070 to 680 grains g^{-1}, with both records remaining low thereafter. This decline coincides with a decrease in the bulk density of the core at ~13 cal ka BP (Fig. 5(b)). A smaller but simultaneous decline is seen in the MD01-2444 pollen concentration record, decreasing from 923.6 to 274.38 grains g^{-1} between ~12 and 11 cal ka BP (Fig. 5(f)). In contrast to our records, the Charco da Candieira lacustrine core shows a significant increase in total pollen concentration from the YD into the Holocene (Van der Knaap and van Leeuwen, 1997), indicating increased vegetation density from the deglaciation into the warmer Holocene interglacial. The SHAK06-5K *ln*(Ca/Ti) reflects variations in the proportion of biogenic (Ca) to detrital (Ti) sediment (Fig. 5(c)) (Hodell *et al.*, 2013b). During warm interglacials/interstadials, Ti has been shown to decrease relative to Ca in the marine environment due to increased vegetation cover, reduced catchment erosion, reduced river transport of detrital material, and also increased carbonate productivity (Hodell *et al.*, 2013b). Our record shows a slight rise in *ln*(Ca/Ti) during the BA and a significant increase throughout the Holocene (Ausín *et al.*, 2020), suggesting a reduced terrigenous supply likely resulting from increased vegetation cover, coinciding with the expansion of woodland.

Consequently, the SHAK06-5K PAR and pollen concentration records would be expected to increase from the glacial into the Holocene, but instead show a significant decline from the middle of the YD into the Holocene, reaching the lowest values in the mid-Holocene (~6.1 cal ka BP). A similar pattern is observed in the total pollen concentration record of nearby marine core MD95-2042 (site shown in Fig. 1; Chabaud *et al.*, 2014), which shows an abrupt decline at ~12 cal ka BP and lowest values between ~8 and 5 cal ka BP. MD01-2444 also documents a reduced pollen concentration from the YD into the Holocene, while core D13882 (Gomes *et al.*, 2020), located on the continental shelf near the mouth of the Tagus (site shown in Fig. S1), shows lower pollen concentrations after 10.6 ka (Fig. 5(g)), remaining low until 5.5 cal ka BP, increasing thereafter.

We suggest that the decline in the pollen concentration and PAR of core SHAK06-5K is a consequence of altered terrestrial sediment deposition at this site. While the source area of pollen to this core site has remained relatively constant over the last 28 ka, the depocentre of terrestrial material delivered from the continent by the Tagus River was altered by rising sea levels over the deglaciation (Jouanneau *et al.*, 1998; Vis *et al.*, 2008, 2016).

Specifically, the decline in the pollen concentration and PAR at our site is coeval with the timing of the disconnection of the Tagus River from the Cascais and Sebútal–Lisbon canyons between 13 and 12 cal ka BP (Vis *et al.*, 2008, 2016; Vis and Kasse, 2009). Throughout MIS 2, the direct connection of the river to these canyons (Fig. S1) meant that high volumes of sediment bypassed the continental shelf and were deposited in the deeper marine environment (Vis *et al.*, 2008, 2016; Vis and Kasse, 2009). Deglacial sea-level rise resulted in the landward movement of the depocentre, starting between 13 and 12 cal ka BP and lasting until 7 cal ka BP (Dias *et al.*, 2000; Vis *et al.*, 2008, 2016; Vis and Kasse, 2009). Consequently, after the disconnection of the canyon with the Tagus River, the transport of pollen to greater depths (including to sites SHAK06-5K and MD01-2444, located on the Promontório do Príncipe de Avis spur) was reduced. High quantities of terrestrial sediment, however, continued to be deposited on the continental shelf until much later; core D13882 (Fig. 1) shows a decline in pollen concentration between 10.6 and 5.1 cal ka BP, coeval with the trapping of large quantities of fluvial sediment in the Lower Tagus Valley which reduced transport to the marine environment (Vis *et al.*, 2016). Once the lower valley had been filled after 5.5 cal ka BP, sedimentation to the shelf increased, which is likely to have contributed to the pollen concentration increase in core D13882 after this time. We therefore suggest that, on a glacial–interglacial timescale, the location of terrestrial sediment deposition in this region, and consequently the PARs at sites SHAK06-5K and MD01-2444, is strongly controlled by relative sea level.

After 2.7 cal ka BP, pollen concentrations and PARs rise slightly, which coincides with a significant rise in SAR and a decline in *ln*(Ca/Ti). Other records from this region also show a rise in sedimentation rates after ~2 cal ka BP, resulting from the impact of anthropogenic land-use change (Vis *et al.*, 2016; Gomes *et al.*, 2020). At the very top of the SHAK06-5K record, after 0.6 cal ka BP, SAR declined, coinciding with reduced
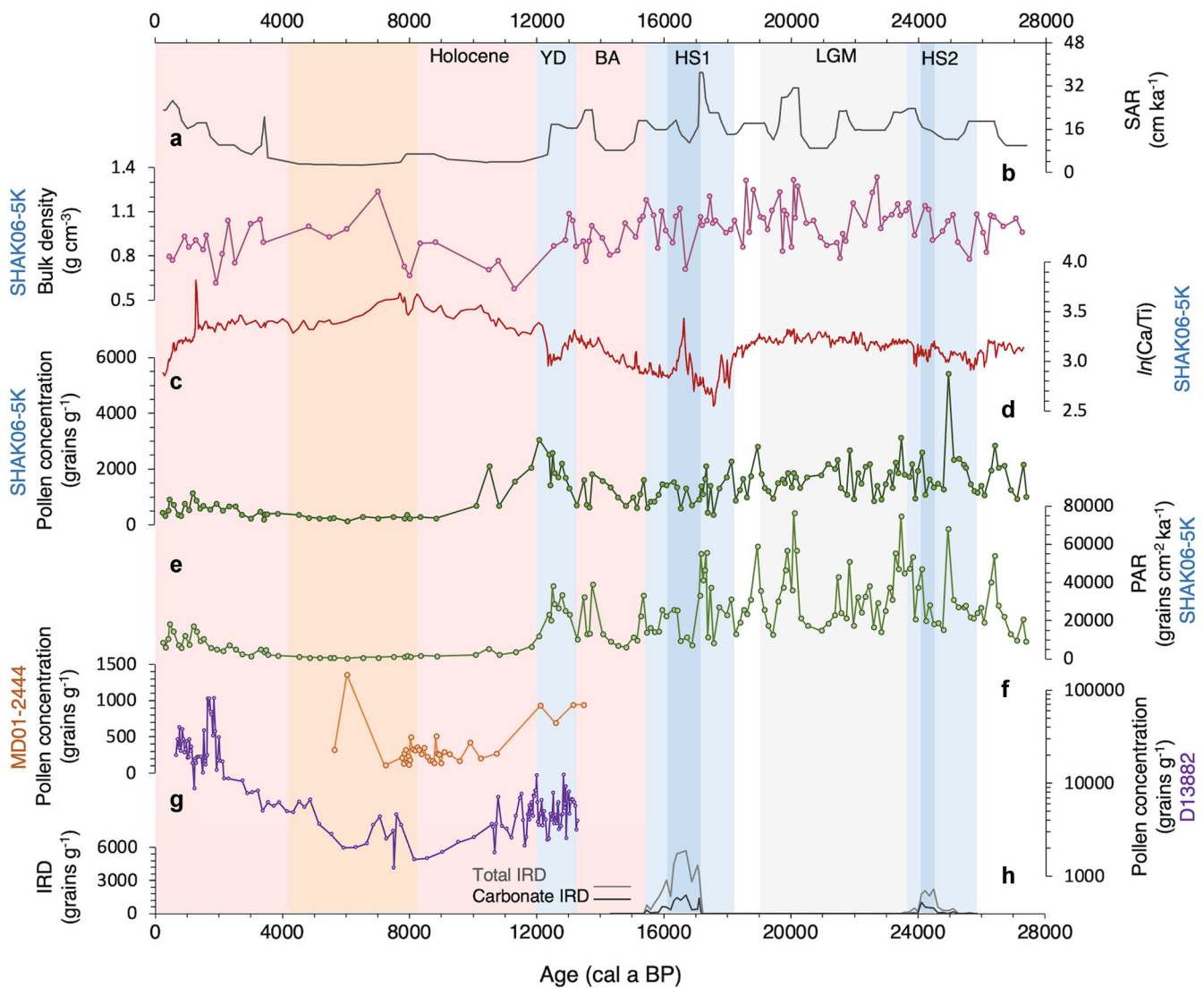
Figure 5. Changes over the past 28 ka (cal a BP) in: (a) sediment accumulation rate of the SHAK06-5K master age model (SAR; cm ka^{-1}); (b) bulk density of core SHAK06-5K (g cm^{-3}); (c) *In*(Ca/Ti) of core SHAK06-5K; (d) pollen concentration of core SHAK06-5K (grains g^{-1}); (e) pollen accumulation rate of core SHAK06-5K (PAR; grains cm^{-2} ka^{-1}); (f) pollen concentration of core MD01-2444 (grains g^{-1}); (g) pollen concentration of core D13882 (Gomes *et al.*, 2020; grains g^{-1}); (h) ice-rafted debris from core SHAK06-5K (grains g^{-1}; Ausín *et al.*, 2020). [Color figure can be viewed at wileyonlinelibrary.com]

PARs and concentrations, a pattern also seen in the pollen concentration of core D13882. This likely reflects the enhanced anthropogenic activities in the catchment after this time (including the intensification of agriculture, reduction of Mediterranean shrubland, establishment of *Pinus* plantations, and hydrological regulation), altering the hydrology and sediment dynamics of the Tagus River (Vis *et al.*, 2008; Fernandes *et al.*, 2020) and consequently altering the deposition of terrestrial material at our core sites.

Orbital-scale variability

Marine Isotope Stage 2

Over MIS 2, the expansion of steppe vegetation, low SSTs (Ausín *et al.*, 2019b; Martrat *et al.*, 2007) and high δ^{18}O$_{G. bulloides}$ values (Ausín *et al.*, 2019a) in core SHAK06-5K as well as high benthic foraminiferal δ^{18}O in MD95-2042 (Shackleton *et al.*, 2000) (Fig. 6), reflect the influence of low insolation, low pCO$_2$, and large northern ice sheets on atmospheric circulation patterns, surface ocean and air temperatures, and on the hydrological cycle (Pollard and Barron, 2003). In addition, this steppe expansion reflects the direct influence of low pCO$_2$ concentrations on the photosynthetic

rate and water use efficiency of vegetation (Polley *et al.*, 1993; Cowling and Sykes, 1999; Ehleringer and Cerling, 1995; Monnin *et al.*, 2001, 2004; Marcott *et al.*, 2014). Research has suggested that the maximum ice-volume extent of the LGM shifted the polar front southwards, intensifying the westerlies over southern Europe and altering the transport of atmospheric heat and moisture (Bard *et al.*, 1987; Eynaud *et al.*, 2009). While some modelling studies have suggested that the westerlies strengthened and shifted southward, and precipitation over the Iberian Peninsula increased during the LGM (Laîné *et al.*, 2009; Beghin *et al.*, 2016; Ludwig *et al.*, 2009; Kutzbach *et al.*, 2020), other simulations show a drying (Braconnot *et al.*, 2007). Simulated cold/dry conditions are in line with the dominance of steppe in vegetation records from this region (Hooghiemstra *et al.*, 1992; Turon *et al.*, 2003; Oliveira *et al.*, 2018).

In the SHAK06-5K record, although steppe elements dominated throughout the LGM, there is a low (<12%) but continuous presence of thermophilous temperate pollen and an increase in Ericaceae pollen percentages which coincides with northern winter at perihelion ~22.5 ka (Fig. 6). Heathland expansion has been linked to reduced summer aridity due to precessional changes leading to reduced boreal summer
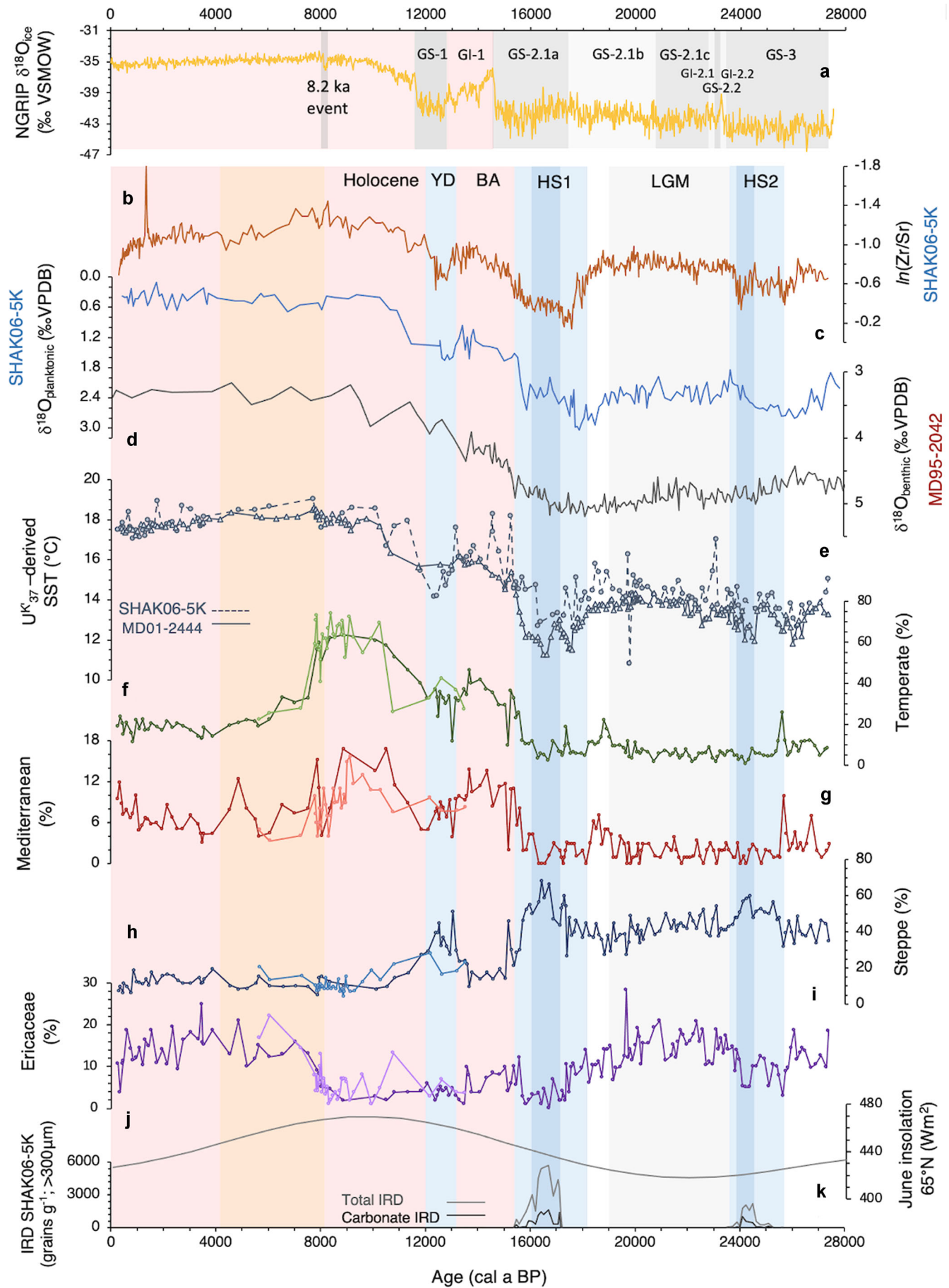
Figure 6   Continued.

insolation (Margari et al., 2007, 2014; Fletcher and Sánchez Goñi, 2008).

While lower LGM temperatures and reduced winter precipitation favoured the expansion of steppe taxa, the reduced seasonality caused by the summer insolation minimum, combined with moderate Iberian Margin SSTs (Cayre et al., 1999; Pailler and Bard, 2002; de Abreu et al., 2003; Ausín et al., 2019b) may have reduced summer evaporative conditions and allowed moderate levels of effective moisture that were able to sustain heathland populations and some thermophilous elements. Simulated precipitation records from western Iberia also show reduced hydrological seasonality during the LGM compared with pre-industrial levels (Menviel et al., 2011).

Early Holocene

Following intermediate expansions and contractions during the Late Glacial (see next section), temperate tree pollen percentages gradually increased at the start of the Holocene, seeing an early expansion of pioneer taxa later replaced by thermophilous temperate elements, indicating an increasingly dense woodland environment and warmer/wetter conditions. Percentages of temperate tree taxa peak in both SHAK06-5K and MD01-2444 between ~10.1 and 8.4 cal ka BP. The gradual forest expansion at the onset of the Holocene is in phase with the gradual decline in $\delta^{18}O_{G.\ bulloides}$ and rise in SSTs. In parallel, Ericaceae percentages declined, reaching a minimum during the time of the summer insolation maximum, associated with enhanced hydrological seasonality and summer aridity, as indicated by the peak in Mediterranean sclerophylls.

What emerges is that while seasonality of precipitation in SW Iberia followed changes in summer insolation, the peak in temperate woodland values lags behind the insolation maximum by ~1–3 ka. Comparison with the timing of vegetation changes during the Last Interglacial (LIG) at the same location (core MD01-2444) (Tzedakis et al., 2018) reveals a distinct difference, with the peak in temperate tree pollen percentages occurring at ~128 ka, very close to the onset of the interglacial and ~1 ka ahead of the insolation peak. One possible explanation for this difference may lie in the evolution of ice volume during the two interglacials, with the sea level approaching (or even exceeding) present-day values at the onset of the LIG (Waelbroeck et al., 2002; Grant et al., 2012; Dutton et al., 2015; Menviel et al., 2019), while being 60 m below present values at the onset of the Holocene (Lambeck et al., 2014) (Fig. 7). Thus, in the early Holocene, residual ice sheets still had a dominant influence over regional temperatures due to the southward deflection of the westerly jet (Harrison et al., 1992; Fletcher et al., 2012), which led to lower SW Iberian surface temperatures and moisture availability, particularly during winter (Baker et al., 2017; Marsicek et al., 2018), which in turn delayed forest expansion, despite maximum boreal insolation.

Early to mid-Holocene transition

At the transition from the early to the mid-Holocene, MD01-2444 displays a brief decline in thermophilous woodland between 8.4 and 7.9 ka, with this contraction extending over the 8.2 ka event, which has been attributed to a catastrophic release of meltwater from Lake Agassiz/Ojibway that led to a perturbation of the AMOC (Barber et al., 1999; Renssen et al., 2001; Alley et al., 2003; Alley andand Ágústsdóttir, 2005; LeGrande et al., 2006) and a large-scale North Atlantic cooling (Von Grafenstein et al., 1998; Tinner and Lotter, 2001; Thomas et al., 2007). After a short recovery, a rapid and significant contraction of thermophilous woodland occurred, declining by ~40% in <500 cal a BP. Temperate woodland percentages remained low (between 19 and 33%) throughout the mid-Holocene, coinciding with an expansion of Ericaceae and heliophilous Cichorioideae. These changes follow the gradual decline in boreal insolation, suggesting that the associated increased summer water availability favoured the expansion of heathland over temperate woodland and provided a more open environment, allowing the expansion of heliophilous elements. While the mid-Holocene gradual expansion of heathland and heliophilous herbs is a relatively linear response to declining boreal insolation, the rapid decline of temperate taxa at ~7.8 cal ka BP signifies an abrupt response to the same gradual climate forcing. This abrupt ecological response will be further explored below (see Intrinsic/extrinsic vegetation change).

Late Holocene

Open woodland characterises the Late Holocene, with low but increasing levels of thermophilous temperate woodland and high levels of heliophilous Cichorioideae and Ericaceae. Iberian Margin SSTs remain high (~17.5°C) (Martrat et al., 2007; Rodrigues et al., 2010; Ausín et al., 2019b; Gomes et al., 2020), although displaying a small gradual decreasing trend from the mid-Holocene. The heathland expansion coincides with a boreal insolation minimum, associated with reduced precipitation seasonality and increased summer water availability. The SHAK06-5K PAR record indicates that anthropogenic activities in the catchment significantly enhanced after 2.7 cal ka BP, while the sharp rise in Pinus after ~0.6 cal ka BP is likely linked to large-scale Pine plantations (van der Knaap and van Leeuwen, 1995).

Abrupt climate variability

Heinrich Stadials 1 and 2

Following Margari et al. (2020), HS2 and HS1 are defined in core SHAK06-5K by changes in lithology: the XRF $ln(Ca/Ti)$ and zirconium/strontium $ln(Zr/Sr)$ ratios (Figs. 5(c) and 6(b)) reflect variations in the relative proportion of detrital (Ti, Zr) and biogenic (Ca, Sr) sediment; this is governed by both dilution by terrigenous sediment and carbonate production. Carbonate productivity during stadial periods declined relative to the supply of terrigenous material; however, transient increases in Ca reflect the input of detrital carbonate associated with ice-rafted debris (IRD), presumably originating from icebergs from the Laurentide ice-sheet, discharged through the Hudson Strait (e.g. Margari et al., 2020).

During HS2 (25.7–23.6 cal ka BP), the pollen spectra are dominated by cryoxerophytic steppe taxa, primarily Artemisia,

Figure 6. Climate records over the past 28 ka (cal a BP) of: (a) North Greenland $\delta^{18}O_{ice}$ established by the Greenland Ice Core Chronology 2005 (VSMOW ‰; Rasmussen et al., 2006, 2014); (b) $ln(Zr/Sr)$ from SHAK06-5K (Ausín et al., 2020); (c) $\delta^{18}O$ of planktonic foraminifera from SHAK06-5K ($\delta^{18}O_{planktonic}$; VPDB ‰; Ausín et al., 2019a); (d) $\delta^{18}O$ of benthic foraminifera from MD95-2042 ($\delta^{18}O_{benthic}$; VPDB ‰; Shackleton et al., 2000); (e) $U^{K'}_{37}$-derived sea surface temperature (SST; °C) from SHAK06-5K (Ausín et al., 2019b) and MD01-2444 (Martrat et al., 2007); (f) temperate pollen from SHAK06-5K (%); (g) Mediterranean pollen from SHAK06-5K (%); (h) steppe pollen from SHAK06-5K; (i) Ericaceae pollen from SHAK05-5K (%); (j) boreal insolation at 65°N (Wm^{-2}; Berger and Loutre, 1991); (k) ice-rafted debris (IRD; grains g^{-1}; Ausín et al., 2020). Note different scales in pollen percentages. The timings of Greenland stadial and Greenland interstadials are established by the Greenland Ice Core Chronology 2005 (GICC05) (Rasmussen et al., 2006; 2014), while the timing of the abrupt transitions in the Iberian Margin records has previously been demarcated in core SHAK06-5K by Ausín et al. (2019a, 2019b) using SST and $\delta^{18}O_{G.\ bulloides}$ records. [Color figure can be viewed at wileyonlinelibrary.com]
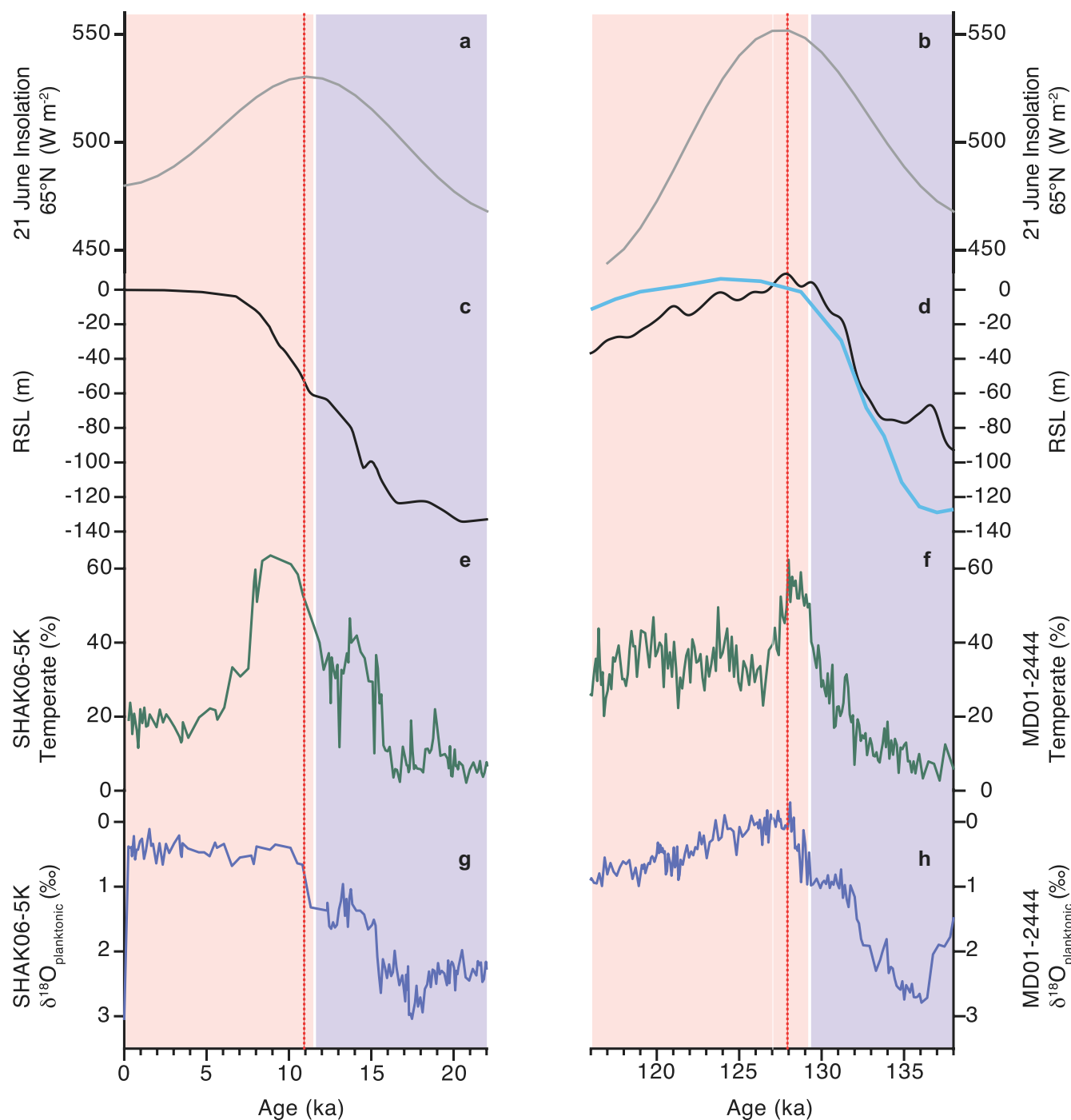
Figure 7. Comparison of Holocene and Last Interglacial deglaciations. (a) and (b) Daily insolation 21 June at 65°N (Berger and Loutre, 1991); (c) relative sea level (RSL) for the last deglaciation and Holocene (Lambeck *et al.*, 2014); (d) RSL for penultimate deglaciation and Last Interglacial (LIG) (black curve: sea-level reconstruction based on Red Sea isotopes (Grant *et al.*, 2012 and modified by Menviel *et al.*, 2019); blue curve: eustatic sea-level record based on benthic foraminiferal isotopes (Waelbroeck *et al.*, 2002)); (e) temperate tree pollen record SHAK06-5K (this study); (f) temperate tree pollen record from MD01-2444 (Tzedakis *et al.*, 2018); (g) planktonic $\delta^{18}O$ record from SHAK06-5K (Ausín *et al.*, 2019a); (h) planktonic $\delta^{18}O$ record from MD01-2444 (Tzedakis *et al.*, 2018). Vertical dotted lines denote insolation maxima, while transitions between coloured boxes denote the onset of the Holocene and the LIG, at 11.7 ka and ~129 ka, respectively. [Color figure can be viewed at wileyonlinelibrary.com]

with some open woodland elements, indicating cold/dry conditions. Early in HS2, an expansion of steppe taxa with the presence of temperate and pioneer vegetation signifies cool temperatures and moderate moisture availability. Within HS2, a small peak in IRD, which includes detrital carbonate, occurs between ~24.6 and 24.1 cal ka BP (Ausín *et al.*, 2020) (Fig. S4i) coeval with a local maximum in steppe taxa, while arboreal taxa and Ericaceae declined, indicating the coldest and driest conditions of the stadial.

HS1 (18.2–15.4 cal ka BP) is a complex interval characterised by lower SSTs, an increase in $\delta^{18}O_{G.\ bulloides,}$ and high steppe

pollen percentages. Early in HS1 (18.2–17.2 cal ka BP), SSTs and pollen percentages of temperate trees and pioneer taxa fluctuate, while Ericaceae remained relatively high. The most extreme conditions of the entire 27.4 cal ka BP record are documented within the second part of HS1, coeval with a peak in IRD, including detrital carbonate (17.2–16.1 cal ka BP): SSTs reached a minimum of ~11°C (Fig. S4c), while the pollen record shows the greatest expansion of steppe taxa alongside minimal levels of temperate and pioneer vegetation and low levels of Ericaceae, signifying the coldest, driest conditions of the stadial and entire deglaciation. In the final section of HS1

(16.1–15.4 cal ka BP), IRD concentrations declined while SSTs and temperate tree pollen percentages gradually recovered, reflecting an interval of slowly evolving conditions before the onset of the BA interstadial.

A complex structure, with a double IRD peak and attendant cooling, has been identified in North Atlantic records of HS1 (Bond and Lotti, 1995; Abrantes et al., 1998; Bard et al., 2000; Marcott et al., 2011; Martrat et al., 2014; Hodell et al., 2017). This has also been observed in SW Iberian Margin SSTs (Pailler and Bard, 2002; Martrat et al., 2007) and primary productivity (Ausín et al., 2020), as well as in northwestern Iberian vegetation records (Naughton et al., 2007, 2009). Our records also show two SST minima at 17.5 and 16.6 cal ka BP, with the first SST decline and SW Iberian steppe expansion occurring prior to the deposition of IRD at our core site. The IRD layer is associated with the second and more extensive SST minimum and steppe maximum, indicating that the penetration of iceberg meltwater at the SW Iberian Margin altered surface ocean conditions and regional hydrology (Bard et al., 2000; Pailler and Bard, 2002; Voelker et al., 2009; Salgueiro et al., 2014; Ausín et al., 2020), leading to the coldest/driest land conditions in SW Iberia. Although the low North Atlantic SSTs during the Heinrich Stadials have been linked to the southward shift in the polar front and strengthened winds over SW and central Iberia (Costas et al., 2016; Wolf et al., 2018, 2019), we suggest that despite the strengthened westerlies, lower regional temperatures reduced evaporation from the ocean, favouring the expansion of steppe taxa during both HS2 and HS1. During both Heinrich Stadials, changes in steppe taxa are in phase with SSTs, $\delta^{18}O_{G.\ bulloides}$ and IRD (Fig. 6), demonstrating a close regional coupling of land–sea conditions in SW Iberia during these extreme cold North Atlantic events.

Bølling–Allerød

The BA (15.4–13.2 cal ka BP) is defined by a change in lithology, with lower XRF ln(Zr/Sr) values than HS1, and is characterised by a shift in SSTs, $\delta^{18}O_{G.\ bulloides}$, and pollen percentages to an interstadial state, indicating warmer and wetter conditions. After a rapid expansion of arboreal vegetation and decline in $\delta^{18}O_{G.\ bulloides}$ at the transition from HS1, temperate taxa briefly declined at 15.2 cal ka BP, coeval with a small decrease in SSTs. Temperate tree values then gradually increased, signifying progressively warmer/wetter conditions, and coinciding with declining $\delta^{18}O_{G.\ bulloides}$. The peak in percentages of thermophilous elements occurred at 13.7 cal ka BP (47%), coeval with a decline in steppe values and rise in SSTs. Ericaceae pollen percentages expanded at the onset of the BA before gradually decreasing, while values of Mediterranean sclerophylls show an opposite trend, suggesting a gradual rise in summer aridity. All arboreal elements declined after 13.7 cal ka BP, along with a contraction of heathland and expansion of steppe, indicating a cooling/drying.

Younger Dryas

The YD event is defined in core SHAK06-5K by changes in lithology (Figs. 5(c) and 6(b)); a shift in XRF ln(Ca/Ti) and ln(Zr/Sr) values demarcates the YD stadial in both cores SHAK06-5K and MD01-2444 (13.2–12 cal ka BP), with the stadial characterised by a drop in SSTs. Their pollen records document the expansion of steppe communities throughout this period, with a moderate presence of mixed open woodland, indicating cooler/drier conditions than the preceding interstadial. The pollen values of steppe taxa, however, do not reach those of HS2 and HS1 and the low but continuous

presence of Mediterranean vegetation suggests that winter temperatures were moderate enough to sustain these elements. At the onset of the YD, steppe taxa rapidly expanded in <250 years, coinciding with a decline in SSTs and a rise in $\delta^{18}O_{G.\ bulloides}$.

Intrinsic/extrinsic vegetation change

For each climate transition (the onset and end of HS2, HS1 and the YD) and the HS1 IRD event, the criteria for abrupt change are met by at least one of the three regional climate records (simulated DJF SAT and annual precipitation and $U^{K'}_{37}$-derived SSTs from MD01-2444); additionally, while not always having two consecutive samples above the threshold for inclusion, some of the records had one data point above 1σ at these transitions (highlighted by blue markers in Fig. 8). This demonstrates that all these climate changes can be defined as abrupt. In the vegetation records, however, the criteria for an abrupt change were not met for all transitions; notably at the onset of HS1 and the transition from the YD into the Holocene. At the onset of HS1 and the Holocene, an abrupt decline is seen in the climate records, while the vegetation records demonstrate a more gradual change.

The highest RoC values for the climate forcing and inferred vegetation response that meet the criteria for abrupt change are shown in Table 4. At the onset of HS2, the RoC of simulated annual precipitation qualifies as an abrupt event, coinciding with an abrupt change in both temperate and steppe pollen. At the end of HS2, the RoC of the declining simulated DJF SAT qualifies as an abrupt event, with the steppe pollen record also demonstrating an abrupt reduction at this time. The onset of HS1 sees an abrupt decline in DJF SAT and SSTs with the latter demonstrating the largest RoC. The pollen records, however, demonstrate a more gradual change at this transition, with the RoC of the temperate and steppe pollen not exceeding the 1σ threshold. The rapid decline in SSTs in the middle of HS1 qualifies as an abrupt event, coinciding with the maximum IRD deposition at this site. In parallel, steppe abruptly increased. Contrary to SW Iberian Margin palaeoceanographic records during HS1 (Bard et al., 2000; Pailler and Bard, 2002; Martrat et al., 2007; Ausín et al., 2020), neither of the simulated records show this event, due to the timing of the freshwater fluxes applied in the model (Fig. 8). At the end of HS1, all regional climate variables show an abrupt change, with the SST record having the largest RoC. This coincides with an abrupt increase in temperate pollen and abrupt decline in steppe taxa, with the latter exhibiting the highest RoC. At the onset of the YD, an abrupt decline is shown in both the simulated annual precipitation and DJF SAT records, with the former having the highest RoC. At this transition, a decline is apparent in the temperate pollen record, which coincides with a marked rise in steppe taxa. At the end of the YD, a rapid decline is shown in both simulated variables but no abrupt change is evident in any of the proxy records. Instead, SSTs and temperate pollen show a gradual rise from the YD into the Holocene, while steppe taxa gradually decline. In the mid-Holocene, the rapid decline in thermophilous woodland between 7 and 7.6 cal ka BP meets the abrupt change criteria. The regional climate records, however, show no abrupt change at this time; while the RoC of SW Iberian SSTs does not exceed the threshold between 9.2 cal ka BP and the late Holocene, the RoC of simulated annual precipitation and DJF SAT does not exceed 1σ for the entire early and mid-Holocene.

In the glacial part of the record, all qualifying abrupt pollen changes in core SHAK06-5K occur either at the transition between stadial and interstadial conditions or at the start/end
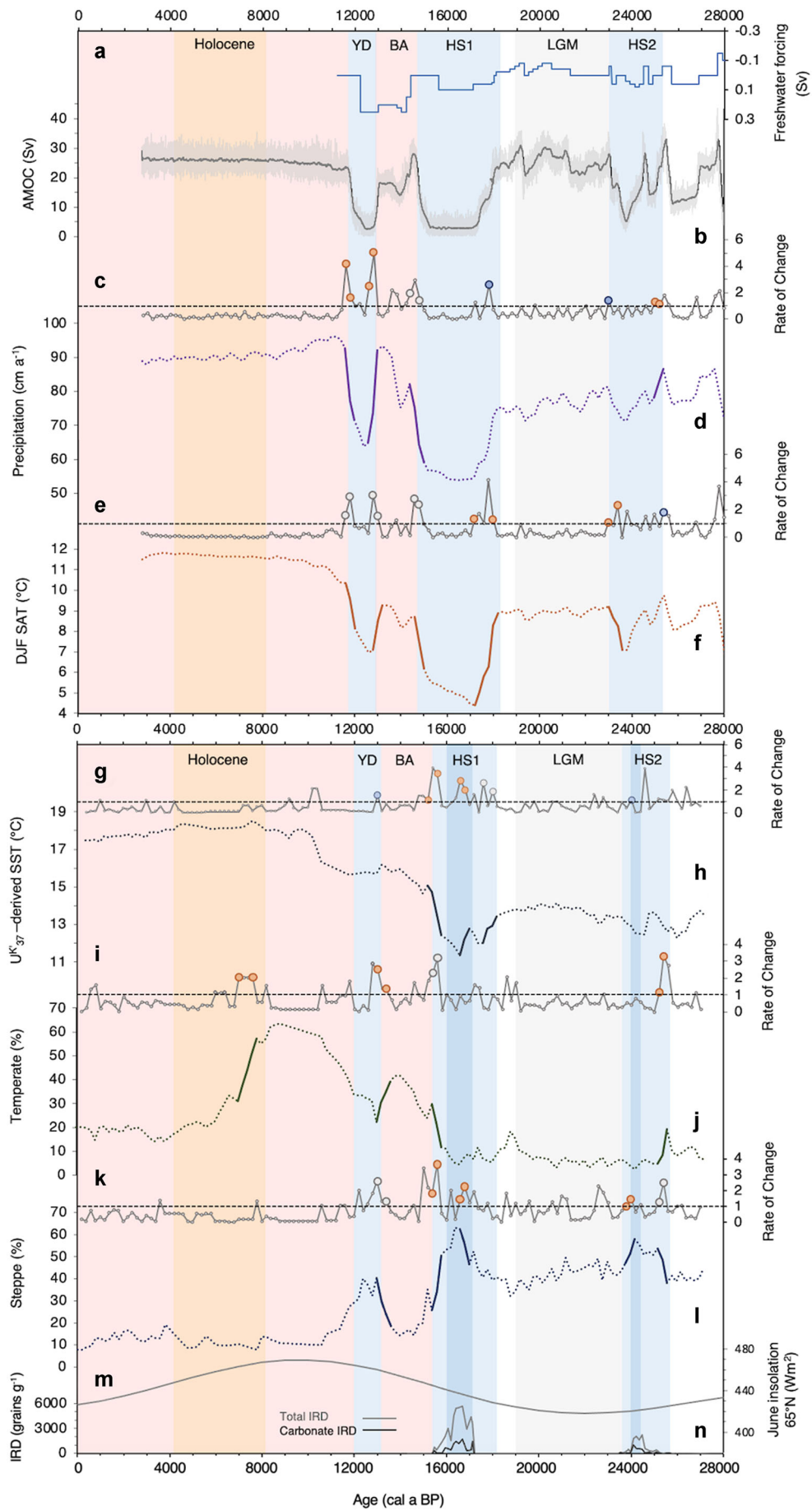
Figure 8   Continued.

of the HS1 IRD event. At all these transitions (the onset and end of HS2, the IRD event during HS1, the end of HS1 and the onset of the YD), these rapid pollen changes coincide with an abrupt change in one or more of the regional climate records (Fig. 8 and Table 4), indicating that these vegetation changes were an ecological response to extrinsic climate changes. The strong weakening or even shutdown of the AMOC during HS2, HS1 and the YD led to SST decrease off the Iberian Margin and in the North Atlantic, due to reduced meridional ocean heat transport (McManus et al., 1999; Martrat et al., 2007). This induced reduced precipitation over Iberia through large-scale atmospheric circulation reorganisation, with stronger anti-cyclonic circulation over southern Europe (e.g. Stockhecke et al., 2016). The sharp decline in temperate tree pollen percentages during the mid-Holocene (7.6–7 cal ka BP), however, does not correspond with an abrupt climate change in any of the climate records. This suggests that the rapid decline in thermophilous woodland was an intrinsically mediated response, whereby temperate woodland crossed an ecological threshold resulting from regional feedback to external conditions. While anthropogenic activity on the Iberian Peninsula dates back ~7.5 ka, anthropogenic disturbance and fire activity in the western Mediterranean at this time was minor and did not peak until ~5.5 ka (van der Knaap and van Leeuwen, 1995; Connor et al., 2019). Consequently, we propose that this threshold was likely to be triggered by the gradual decline in boreal insolation and its influence on precipitation seasonality.

Comparison with existing vegetation records

Here, we compare four existing high-resolution SW Iberian pollen records, covering various stages of the last 28 cal ka BP, with those of SHAK06-5K and MD01-2444 (Fig. 9). The locations of these cores are shown in Fig. 1. Three of these are marine cores located close to the mouth of the Tagus River, while one is a lacustrine record from Charco da Candieira in the Serra da Estrela, Portugal (van der Knaap and van Leeuwen, 1995, 1997), located 1400 m a.s.l., bordering the Tagus catchment basin. While the marine records display large-scale

vegetation change across this region, the terrestrial record documents a regional signal (which includes local vegetation through to extra-regional vegetation over tens of kilometres away from the site) (van der Knaap and van Leeuwen, 1995), and provides a sense of spatial heterogeneity in the region. It must be noted that pollen percentages from the marine and terrestrial cores are not directly comparable. This is because in Iberian Margin pollen records, herbaceous pollen percentages (from riparian and coastal vegetation communities) are often overrepresented, while Pinus is excluded from the pollen sum.

The pollen records from marine cores SHAK06-5K and U1385 (Oliveira et al., 2018) cover HS1 and demonstrate the dominance of steppe taxa, reaching 68% in SHAK06-5K and 50% in U1385, indicating cold/dry conditions. Temperate forest and Ericaceae values remained low, while Pinus percentages were high over this stadial. The BA is covered in both SHAK06-5K and U1385, while MD95-2042 (Chabaud et al., 2014) begins in the mid-BA. The Charco da Candieira pollen record was plotted against a new age model, using the 24 ^{14}C bulk dates from the same record (van der Knaap and van Leuween, 1995, 1997) and calibrated in Oxcal using the Intcal20 calibration curve (Reimer et al., 2020). According to this, the record covers the interval 14.3–0.4 cal ka BP and shows high percentages of temperate taxa during the BA (~22%), signifying warmer/wetter conditions (Fig. 9). The other records also show high levels of temperate taxa throughout the BA, averaging ~45% in U1385 and ~34% in SHAK06-5K. A small rise in Ericaceae is documented in both SHAK06-5K and the Charco da Candieira record, indicating a slight rise in year-round moisture availability coinciding with high lake levels in the Serra da Estrela region (van der Knaap and van Leuween, 1997). An abrupt decline in temperate taxa and rise in steppe vegetation is seen in all cores at the transition from the BA into the YD, signifying a rapid regional cooling/drying. Lake levels are low in the Serra da Estrela region (van der Knaap and van Leuween, 1997), while on average, steppe percentages are ~36% in SHAK06-5K, ~24% in MD95-2042, ~24% in U1385, ~3% in Charco da Candieira and ~20% in D13882 (Gomes et al., 2020). All records document a gradual expansion of thermophilous temperate forest during the early Holocene,

Table 4. Rate of change (RoC) of regional climate forcings (annual precipitation (cm a^{-1}) and surface air temperatures for December, January and February (DJF SAT) (°C) over western Iberia, and southwestern Iberian Margin sea surface temperatures (SSTs) from MD01-2444 (°C)), and southwestern Iberian vegetation (steppe/temperate taxa) at the transitions of the millennial-scale climate events over the past 28 ka.

		Climate variable			Pollen change		
		Age (ka BP)	RoC	Forcing	Age (ka BP)	RoC pollen	Inferred vegetation type
Heinrich Stadial 2	Onset	25–25.2	1.18	Precipitation	25.2–25.4	2.24	Temperate
	End	23–23.4	1.41	DJF SAT	23.8–24	1.23	Steppe
Heinrich Stadial 1	Onset	17.2–18	1.89	DJF SAT	-	-	-
	IRD event	16.6–16.8	2.45	SST	16.6–16.8	1.86	Steppe
	End	15.2–15.6	2.83	SST	15.4–15.6	2.76	Steppe
Younger Dryas	Onset	12.6–12.8	3.74	Precipitation	13–13.4	1.76	Temperate
	End	11.6–11.8	2.87	Precipitation	-	-	-
Holocene		-	-	-	7–7.6	2.04	Temperate

Figure 8. Changes over time (cal ka BP) in: (a) added freshwater forcing into the North Atlantic (Sv); (b) simulated AMOC (Sv) (grey) smoothed with 100-year running mean (black line); (c) and (d) the normalised rates of change and resampled climate and vegetation records of simulated annual precipitation (cm a^{-1}); (e) and (f) simulated December to February surface air temperature (DJF SAT; °C); (g) and (h) U$^{K'}_{37}$-derived sea surface temperatures from MD01-2444 (SST; °C). MD01-2444 SSTs were aligned to the master age model using the automated proxy-to-proxy stratigraphical alignment method outlined in the text; (i) and (j) temperate taxa from SHAK06-5K (%); (k) and (l) steppe taxa from SHAK06-5K (%); and changes in time of (m) boreal insolation at 65°N (Wm^{-2}; Berger and Loutre, 1991); (n) ice-rafted debris (IRD; grains g^{-1}; Ausín et al., 2020). For the climate records, dashed lines illustrate the entire record while the solid lines show the abrupt transitions. Orange and grey markers highlight the values of RoC for the climate forcing and inferred vegetation response that meet the criteria for abrupt change; the former demonstrates the climate/pollen record with the highest RoC. Blue markers highlight single data points at the transitions that exceed 1σ, but do not meet the criteria for abrupt change. The climate model and proxy records have different timescales and are therefore displayed separately. [Color figure can be viewed at wileyonlinelibrary.com]
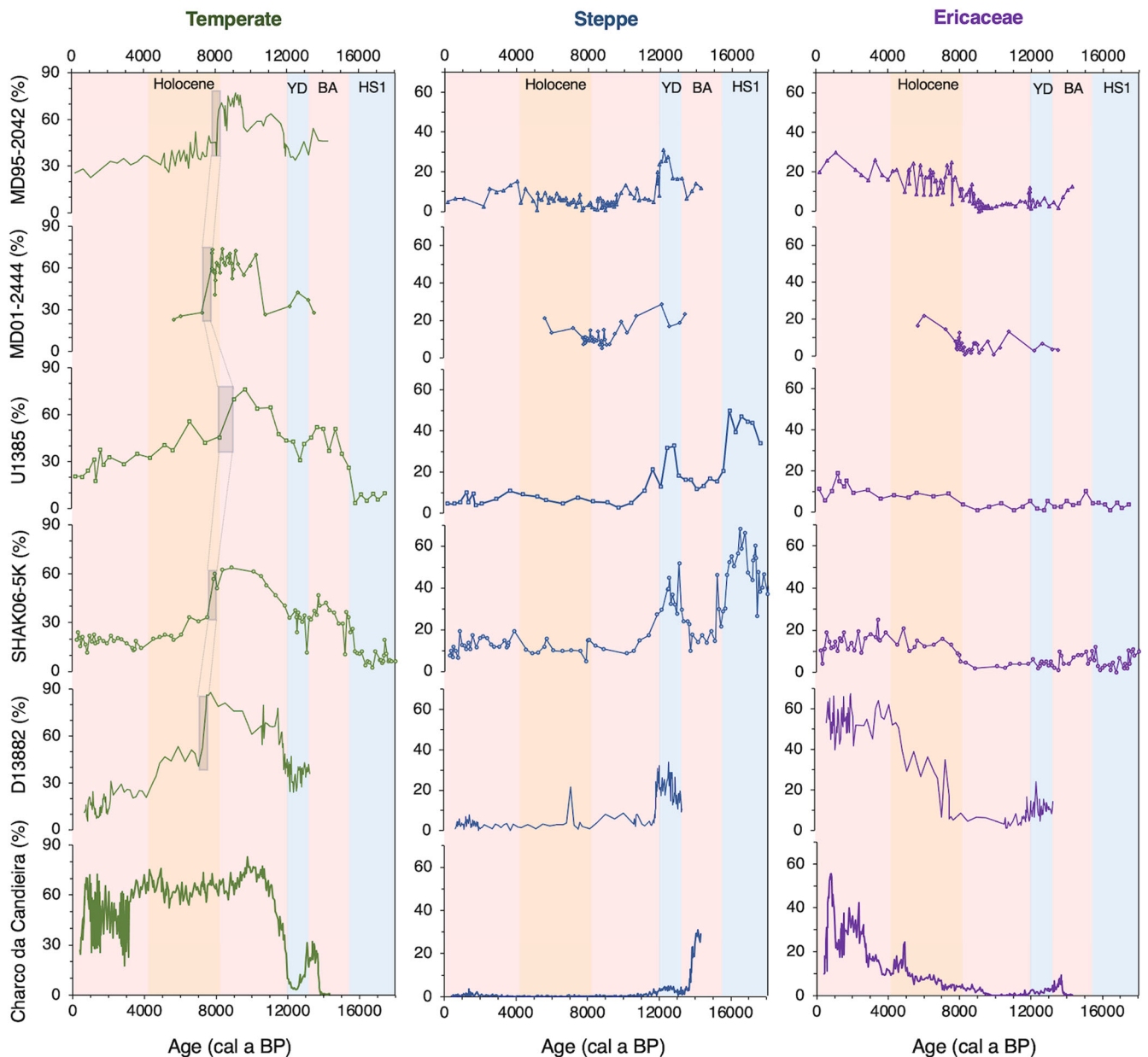
Figure 9. Southwestern Iberian pollen records of temperate tree (green), steppe (blue), and Ericaceae (purple) vegetation change over the last deglaciation and Holocene, from cores MD95-2042 (Chabaud *et al.*, 2014), MD01-2444 (this study), U1385 (Oliveira *et al.*, 2018), SHAK06-5K (this study), D13882 (Gomes *et al.*, 2020) and Charco da Candieira (Van der Knaap and van Leeuwen, 1997). Shaded areas and dashed lines correspond to the abrupt change in temperate taxa during the mid-Holocene. All records have been plotted against their respective age models, with the exception of Charco da Candieira, which has been plotted using a new age model produced using the 24 ^{14}C bulk dates from the same record and calibrated in Oxcal using the Intcal20 calibration curve. [Color figure can be viewed at wileyonlinelibrary.com]

with the peak in these elements occurring between 9.7 and 8.8 ka BP in the SHAK06-5K, MD95-2042, U1385 and Charco da Candieira records. The timing of this maximum woodland expansion coincides with increased lake levels in the Serra da Estrela region (van der Knaap and van Leuween, 1997). In core D13882, the peak in temperate woodland occurs later, at ~7.6 cal ka BP. The maximum percentage of these elements ranges between 64% in SHAK06-5K and 88% in the Charco da Candieira core, with all records indicating that optimal conditions for forest expansion occurred around ~2 cal ka BP after the peak in insolation. After the peak in woodland, thermophilous elements in cores SHAK06-5K, MD01-2444 and MD95-2042 briefly decline. Dated at ~8.6 cal ka BP in MD95-2042, and given age uncertainties, it is likely that this event is aligned with the 8.2 cal ka BP decline displayed in cores SHAK06-5K and MD01-2444. These three cores, therefore, imply a response of SW Iberian vegetation to regional

cooling associated with feedback resulting from the 8.2 ka event. The lower resolution of the other regional pollen records at this time prevents this event from being assessed.

All SW Iberian Margin marine cores analysed here display a rapid and significant decline in thermophilous woodland at the start of the mid-Holocene (~7.8 cal ka BP), with temperate elements declining to 30–45% in less than 500 years (Fig. 9). Since the North Atlantic climate does not display any abrupt changes of this magnitude at this time, vegetation records from this region support the suggestion of an abrupt, intrinsic, non-linear response of SW Iberian thermophilous woodland to the gradual forcing of declining boreal insolation. The Charco da Candieira record, however, does not show this abrupt wood-land contraction. This could be because the bioclimatic setting of this upland site prevented the crossing of an ecological threshold. Another possibility is that this is related to the problem of closure in percentages, where significant changes

in the size of tree populations are barely discernible when arboreal pollen values are high (Magri, 1994).

All late Holocene marine records from this region document low levels of temperate taxa compared with the early interglacial. The high-resolution D13882 and Charco da Candieira records demonstrate significant multi-centennial variability in temperate woodland after 2.2 and 3.2 cal ka BP, respectively, likely due to the increasing intensification of anthropogenic pressures on this region's land use, hydrology and vegetation (van der Knaap and van Leeuwen, 1995; Gomes et al., 2020). A rise in Ericaceae is seen in all cores over the late Holocene, coinciding with the declining boreal insolation, demonstrating the response of heathland to the associated rise in summer water availability. The final peak in the Charco da Candieira record at 0.8 cal ka BP is likely caused by anthropogenic activities (van der Knaap and van Leeuwen, 1995; Tzedakis, 2010), while the heathland expansion after 2 ka in D13882 may also be anthropogenically influenced (Gomes et al., 2020). In the SHAK06-5K, U1385 and Charco da Candieira records, a sharp rise in *Pinus* can be seen after ~0.6 cal ka BP, possibly linked to the large-scale planting of this genus.

In summary, the pollen records discussed here provide support for the presence of both extrinsic ecological responses of SW Iberian vegetation to rapid climate regime shifts during HS2, HS1, the BA and the YD as well as an intrinsic abrupt vegetation response at ~7.8 cal ka BP to gradual climate change.

Conclusions

- Over the deglaciation and Holocene, the terrestrial sediment deposition at the SHAK06-5K/MD01-2444 core sites is strongly influenced by relative sea-level changes. Until ~12 ka BP, the pollen concentration and PAR in SHAK06-5K are relatively high, abruptly declining thereafter resulting from marine transgression and the consequential landward movement of the terrestrial sediment depocentre.
- Comparing the temperate and steppe records from core SHAK06-5K with SSTs, $\delta^{18}O_{G.bulloides}$, and ln(Ca/Ti) from the same core, a clear correspondence is apparent in the timing of orbital and many millennial-scale changes in all records. Additionally, when comparing our pollen records with existing SW Iberian vegetation records, a clear synchroneity can be seen in the timing and magnitude of abrupt vegetation changes in these records, in response to the abrupt climate events of HS2, HS1, the BA and the YD.
- On orbital timescales, over MIS 2 and the onset of the Holocene, changes in temperate tree and steppe pollen percentages from SHAK06-5K document a close coupling with Iberian Margin SSTs, $\delta^{18}O_{G.bulloides}$ and benthic $\delta^{18}O$, demonstrating the influence of North Atlantic conditions and global ice-volume on SW Iberian thermophilous and steppe elements over this period. This influence continues at the onset of the Holocene, likely due to the presence of residual high-latitude ice sheets, causing the thermophilous woodland peak to lag behind the boreal summer insolation maximum by ~2 ka. The same pattern is also apparent in existing SW Iberian Margin Holocene pollen records and contrasts with that from the LIG where the thermophilous peak was reached before the boreal summer insolation maximum.
- Over MIS 2, on millennial timescales, the rapid changes in thermophilous and steppe elements in SHAK06-5K and MD01-2444 (at the onset and end of HS2, the IRD event and

end of HS1, and the onset of the YD) are synchronous with abrupt North Atlantic events. The synchroneity and high RoC of these transitions in both the vegetation and regional climate records suggests that these abrupt vegetation changes are extrinsically forced. At ~7.8 cal ka BP, our pollen records demonstrate an abrupt and significant decline in thermophilous woodland, a pattern that is also documented in existing vegetation records from this region. Occurring while boreal insolation is in gradual decline and North Atlantic conditions are relatively stable, this demonstrates an intrinsically mediated abrupt vegetation response, signifying that temperate taxa crossed an ecological threshold, possibly resulting from changing moisture availability resulting from altered precipitation seasonality.

Supporting information

Additional supporting information can be found in the online version of this article.

Supporting information.

References

Abe-Ouchi A, Segawa T, Saito F. 2007. Climatic Conditions for modelling the Northern Hemisphere ice sheets throughout the ice age cycle. *Climate of the Past* **3**: 423–438.

Abrantes F. 1992. Palaeoproductivity oscillations during the last 130 ka along the Portuguese and NW African margins. *Geological Society* **64**: 499–510.

Abrantes F, Baas J, Haflidason H et al. 1998. Sediment fluxes along the northeastern European Margin: inferring hydrological changes between 20 and 8 kyr. *Marine Geology* **52**: 7–23.

Aguiar FC, Ferreira MT, Moreira IS et al. 2000. Riparian types on a Mediterranean basin. *Aspects of Applied Biology* **58**: 221–232.

Aguiar FC, Ferreira MT. 2005. Human-disturbed landscapes: effects on composition and integrity of riparian woody vegetation in the Tagus River basin, Portugal. *Environmental Conservation* **32**: 30–41.

Ahn J, Brook EJ. 2014. Simple Dome ice reveals two modes of millennial CO2 change during the last ice age. *Nature Communications* **5**: 1–6.

Alley RB, Mayewski PA, Sowers T et al. 1997. Holocene climatic instability: A prominent, widespread event 8200 yr ago. *Geology* **25**: 483.

Alley RB, Marotzke J, Nordhaus WD et al. 2003. Abrupt Climate Change. *Science* **299**: 2005–2010.

Alley RB, Ágústsdóttir AM. 2005. The 8k event: cause and consequences of a major Holocene abrupt climate change. *Quaternary Science Reviews* **24**: 1123–1149.

Ambar I, Fiúza A. 1994. Some features of the Portugal current system: a poleward slope undercurrent, an upwelling-related summer southward flow and an autumn-winter poleward surface current. In *Proceedings of the second international conference on air-sea interaction and on meteorology and oceanography of the coastal zone*, Katsaros KB, Fiúza A, Ambar I (eds.). American Meteorological Society: Boston, MA; 286–287.

Arzola RG, Wynn RB, Lastras G et al. 2008. Sedimentary features and processes in the Nazaré and Setúbal submarine canyons, west Iberian margin. *Marine Geology* **250**: 64–88.

Ausín B, Haginpour N, Wacker L et al. 2019a. Radiocarbon age offsets between two surface dwelling planktonic foraminifera species during abrupt climate events in the SW Iberian Margin. *Paleoceanography & Paleoclimatology* **34**: 63–78.

Ausín B, Magill C, Haghipour N et al. 2019b. (In)coherent multiproxy signals in marine sediments: Implications for high-resolution paleoclimate reconstruction. *Earth & Planetary Science Letters* **515**: 38–46.

Ausín B, Hodell DA, Cutmore A et al. 2020. The impact of abrupt deglacial climate variability on productivity and upwelling on the southwestern Iberian Margin. *Quaternary Science Reviews* **230**: 1–13.

Ausín B, Sarnthein M, Haghipour N. 2021. Glacial-to-deglacial reservoir and ventilation ages on the southwest Iberian continental margin. *Quaternary Science Reviews* **225**: 1–11.

Baker JL, Lachniet MS, Chervyatsova O et al. 2017. Holocene warming in western continental Eurasia driven by glacial retreat and greenhouse forcing. *Nature Geoscience* **10**: 430–435.

Barber DC, Dyke A, Hillaire-Marcel C et al. 1999. Forcing of the cold event of 8,200 years ago by catastrophic drainage of Laurentide lakes. *Nature* **400**: 344–348.

Bard E, Arnold A, Maurice P et al. 1987. Retreat velocity of the North Atlantic polar front during the last deglaciation determined by 14C accelerator mass spectrometry. *Nature* **328**: 791–794.

Bard E, Rostek F, Turin J-L et al. 2000. Hydrological Impact of Heinrich Events in the Subtropical Northeast Atlantic. *Science* **289**: 1321–1324.

Bard E, Tuna T, Fagault Y et al. 2015. AixMICADAS, the accelerator mass spectrometer dedicated to 14C recently installed in Aix-en-Provence, France. *Nuclear Instruments and Methods in Physics Research B* **361**: 80–86.

Barker S, Diz P, Vautravers MJ et al. 2009. Interhemispheric Atlantic seesaw response during the last deglaciation. *Nature* **457**: 1097–1102.

Bell BA, Fletcher WJ. 2016. Modern surface pollen assemblages from the Middle and High Atlas, Morocco: insights into pollen representation and transport. *Grana* **55**: 286–301.

Beghin P, Charbit S, Kageyama M et al. 2016. What drives LGM precipitation over the western Mediterranean? A study focused on the Iberian Peninsula and northern Morocco. *Climate Dynamics* **46**: 2611–2631.

Bennett KD 2011. Psimpoll and pscomb programs for plotting and analysis. http://chrono.qub.ac.uk/psimpoll/psimpoll.html [accessed 20 December 2021].

Berger A. 1978. Long-term variations of daily insolation and quaternary climatic changes. *Journal of Atmospheric Science* **35**: 2362–2367.

Berger A, Loutre MF. 1991. Insolation values for the climate of the last 10 million years. *Quaternary Science Reviews* **10**: 297–317.

Beug HJ 2004. Leitfaden der Pollenbestimmung fur Mitteleuropa und angrenzende Gebiete. Verlag Friedrich Pfeil: Munich.

Blanco Castro E, Casado Gonzalez MA, Costa, Tenorio M et al. 1997. Los bosques ibericos: Una interpretacion geobotanica. Planeta: Barcelona.

Bond G, Heinrich H, Broecker W et al. 1992. Evidence for massive discharges of icebergs into the North Atlantic Ocean during the last glacial period. *Nature* **360**: 245–249.

Bond G, Lotti R. 1995. Iceberg discharges into the North Atlantic on millennial time scales during the last glaciation. *Science* **267**: 1005.

Bond G, Showers W, Cheseby M et al. 1997. A Pervasive Millennial-Scale Cycle in North Atlantic Holocene and Glacial Climates. *Nature* **278**: 1257–1266.

Braconnot P, Otto-Bliesner B, Harrison S et al. 2007. Results of PMIP2 coupled simulations of the Mid-Holocene and Last Glacial Maximum – Part 1: experiments and large-scale features. *Climate of the Past* **3**: 261–277.

Broecker W, Bond G, Klas M et al. 1992. Origin of the northern Atlantic's Heinrich events. *Climate Dynamics* **6**: 265–273.

Bronk Ramsey C. 2007. Deposition models for chronological records. *Quaternary Science Reviews* **27**: 42–60.

Bronk Ramsey C. 2009. Bayesian Analysis of Radiocarbon Dates. *Radiocarbon* **51**: 337–360.

Cayre O, Lancelot Y, Vincent E et al. 1999. Paleoceanographic reconstructions from planktonic foraminifera off the Iberian Margin: Temperature, salinity, and Heinrich events. *Palaeogeography, Palaeoclimatology, Palaeoecology* **14**: 384–396.

Chabaud L, Sánchez Goñi MF, Desprat S et al. 2014. Land–sea climatic variability in the eastern North Atlantic subtropical region over the last 14,200 years: Atmospheric and oceanic processes at different timescales. *The Holocene* **24**: 787–797.

Connor SE, Vannière B, Colombaroli D et al. 2019. Humans take control of fire-driven diversity changes in Mediterranean Iberia's vegetation during the mid–late Holocene. *The Holocene* **29**: 886–901.

Costas S, Naughton F, Goble R et al. 2016. Windiness spells in SW Europe since the last glacial maximum. *Earth & Planetary Science Letters* **436**: 82–92.

Cowling SA, Sykes MT. 1999. Physiological Significance of Low Atmospheric CO_2 for Plant–Climate Interactions. *Quaternary Research* **52**: 237–242.

Dansgaard W, Clausen HB, Gundestrup N et al. 1982. A new Greenland deep ice core. *Science* **218**: 1273–1277.

Dansgaard W, Johnsen SJ, Clausen HB et al. 1993. Evidence for general instability of past climate from a 250-kyr. *Nature* **364**: 218–220.

de Abreu L, Shackleton NJ, Schönfeld J et al. 2003. Millennial-scale oceanic climate variability off the Western Iberian margin during the last two glacial periods. *Marine Geology* **196**: 1–20.

de Stigter HC, Jesus CC, Boer W et al. 2011. Recent sediment transport and deposition in the Lisbon–Setúbal and Cascais submarine canyons, Portuguese continental margin. *Deep-Sea Research II* **58**: 2321–2344.

Denton GH, Broecker WS, Alley RB. 2006. The mystery interval 17.5 to 14.5 kyrs ago. *PAGES News* **14**: 14–16.

Dias JMA, Boski T, Rodrigues A et al. 2000. Coast line evolution in Portugal since the Last Glacial Maximum until present—a synthesis. *Marine Geology* **170**: 177–186.

Dutton A, Carlson AE, Long AJ et al. 2015. Sea-level rise due to polar ice-sheet mass loss during past warm periods. *Science* **349**: 153–165.

Ehleringer JR, Cerling TE. 1995. Atmospheric CO_2 and the ratio of intercellular to ambient CO_2 concentrations in plants. *Tree Physiology* **15**: 105–111.

Eynaud F, de Abreu L, Voelker A et al. 2009. Position of the Polar Front along the western Iberian margin during key cold episodes of the last 45 ka. *Geochemistry, Geophysics, Geosystems* **10**: 1–21.

Fernandes MR, Aguia FC, Martins MJ et al. 2020. Long-term human-generated alterations of Tagus River: Effects of hydrological regulation and land-use changes in distinct river zones. *Catena* **188**: 1–14.

Fick SE, Hijmans RJ. 2017. WorldClim 2: new 1-km spatial resolution climate surfaces for global land areas. *International Journal of Climatology* **37**: 4302–4315.

Fiúza AFD, DeMacedo ME, Guerreiro MR. 1982. Climatological space and time-variation of the Portuguese coastal upwelling. *Oceanologica Acta* **5**: 31–40.

Fletcher WJ, Sánchez Goñi MF. 2008. Orbital- and sub-orbital-scale climate impacts on vegetation of the western Mediterranean basin over the last 48,000 yr. *Quaternary Research* **70**: 451–464.

Fletcher WJ, Debret M, Sánchez Goñi MF. 2012. Mid-Holocene emergence of a low- frequency millennial oscillation in western

Mediterranean climate: Implications for past dynamics of the North Atlantic atmospheric westerlies. *The Holocene* **23**: 153–166.

Freeman E, Skinner LC, Waelbroeck C, Hodell D. 2016. Radiocarbon evidence for enhanced respired carbon storage in the Atlantic at the Last Glacial Maximum. *Nature Communications* **7**:

Giorgi F, Lionello P. 2008. Climate change projections for the Mediterranean region. *Global and Planetary Change* **63**: 90–104.

Gomes SD, Flectcher WJ, Rodrigues T et al. 2020. Time-transgressive Holocene maximum of temperate and Mediterranean forest development across the Iberian Peninsula reflects orbital forcing. *Palaeogeography, Palaeoclimatology, Palaeoecology* **550**: 1–16.

Goosse H, Brovkin V, Fichefet T et al. 2010. Description of the Earth system model of intermediate complexity LOVECLIM version 1.2. *Geoscientific Model Development* **3**: 603–633.

Grant K, Rohling E, Bar-Matthews M et al. 2012. Rapid coupling between ice volume and polar temperature over the past 150,000 years. *Nature* **491**: 744–747.

Grimm EC, Jacobson GL. 1992. Fossil-pollen evidence for abrupt climate changes during the past 18 000 years in eastern North America. *Climate Dynamics* **6**: 179–184.

Harrison SP, Prentice IC, Bartlein PJ. 1992. Influence of insolation and glaciation on atmospheric circulation in the North Atlantic sector: Implications of general circulation model experiments for the Late Quaternary climatology of Europe. *Quaternary Science Reviews* **11**: 283–299.

Hartz N, Milthers V. 1901. Det senglaciale ler I Allerod Teglvaerks-grav. *Meddelelser fra Dansk Geologisk Forening* **2**: 31–60.

Heaton TJ, Köhler P, Butzin M et al. 2020. Marine20—The Marine Radiocarbon Age Calibration Curve (0–55,000 Cal BP). *Radiocarbon* **62**: 1–42.

Hodell DA, Lourens L, Stow DAV et al. and the Shackleton Site Project Members 2013a. The "Shackleton Site" (IODP Site U1385) on the Iberian Margin. *Scientific Drilling* **16**: 13–19.

Hodell D, Crowhurst S, Skinner L et al. 2013b. Response of Iberian Margin sediments to orbital and suborbital forcing over the past 420 ka. *Paleoceanography* **28**: 185–199.

Hodell DA, Elderfield H, Greaves M et al. the JC089 Scientific Party. 2014. JC089 Cruise Report- IODP Site Survey of the Shackleton Sites, SW Iberian Margin, British Ocean Data Centre. Available at: https://www.bodc.ac.uk/data/information_and_inventories/cruise_inventory/report/13392/

Hodell DA, Tomaso N, Bontognali RR et al. 2017. Anatomy of Heinrich Layer 1 and its role in the last deglaciation. *Paleoceanography & Paleoclimatology* **32**: 284–303.

Hooghiemstra H, Stalling H, Agwu COC et al. 1992. Vegetational and climatic changes at the northern fringe of the Sahara 250,000–5000 years BP: evidence from 4 marine pollen records located between Portugal and the Canary Islands. *Review of Palaeobotany & Palynology* **74**: 1–53.

Hopkins JS. 1950. Differential Flotation and Deposition of Coniferous and Deciduous Tree Pollen. *Ecology* **31**: 633–641.

Hurrell JW. 1995. Decadal Trends in the North Atlantic Oscillation: Regional Temperatures and Precipitation. *Science* **269**: 676–679.

Jorge da Silva A. 1992. Dependence of upwelling related circulation on wind forcing and stratification over the Portuguese northern shelf. ICES CM2/C 17. *Hydrography Committee: Copenhagen* 1–12.

Jouanneau JM, Garcia C, Oliveira A et al. 1998. Dispersal and deposition of suspended sediment on the shelf off the Tagus and Sado estuaries, SW Portugal. *Progress in Oceanography* **42**: 233–257.

Kreyling J. 2010. Winter climate change: a critical factor for temperate vegetation performance. *Ecology* **91**: 1939–1948.

Kutzbach JE, Guan J, He F et al. 2020. African climate response to orbital and glacial forcing in 140,000-y simulation with implications for early modern human environments. *Proceedings of the National Academy of Sciences* **117**: 2255–2264.

Laîné A, Kageyama M, Salas-Mélia D et al. 2009. Northern hemisphere storm tracks during the last glacial maximum in the PMIP2 ocean-atmosphere coupled models: energetic study, seasonal cycle, precipitation. *Climate Dynamics* **32**: 593–614.

Lamb HF, van der Kaars S. 1995. Vegetational response to Holocene climatic change: pollen and palaeolimnological data from the Middle Atlas. Morocco. *The Holocene* **5**: 400–408.

Lambeck K, Rouby H, Purcell A et al. 2014. Sea level and global ice volumes from the Last Glacial Maximum to the Holocene. *Proceedings of the National Academy of Sciences* **111**: 15296–15303.

Lebreiro SM, Voelker AHL, Vizcaino A et al. 2009. Sediment instability on the Portuguese continental margin under abrupt glacial climate changes (last 60 ka). *Quaternary Science Reviews* **28**: 3211–3223.

LeGrande AN, Schmidt GA, Shindell DT et al. 2006. Consistent simulations of multiple proxy responses to an abrupt climate change event. *Proceedings of the National Academy of Sciences* **103**: 837–842.

Lionello P. 2012. *The Climate of the Mediterranean Region. From the Past to the Future*. Elsevier: Amsterdam.

Lionello P, Abrantes F, Gacic M et al. 2014. The climate of the Mediterranean region: research progress and climate change impacts. *Regional Environmental Change* **14**: 1679–1684.

Loureiro JJ, Machado ML, Macedo ME et al. 1986. Monografias hidrológicas dos principais cursos de água de Portugal continental. Direcção Geral dos Serviços Hidraulicos: Lisbon.

Ludwig P, Schaffernicht EJ, Shao Y, Pinto JG. 2016. Regional atmospheric circulation over Europe during the Last Glacial Maximum and its links to precipitation. *Journal of Geophysical Research: Atmospheres*, **121**: 2130–2145. http://doi.org/10.1002/2015jd024444

Mabberley DJ. 2017. *Mabberley's Plant-book: A Portable Dictionary of Plants, their Classification and Uses*. 4th ed. Cambridge University Press: Cambridge.

Magny M, Thew N, Hadorn P. 2003a. Late-glacial and early Holocene changes in vegetation and lake-level at Hauterive/Rougest-Terres, lake Neuchâtel (Switzerland). *Journal of Quaternary Science* **18**: 31–40.

Magny M, Bégeot C, Guiot J et al. 2003b. Contrasting patterns of hydrological changes in Europe in response to Holocene climate cooling phases. *Quaternary Science Reviews* **22**: 1589–1596.

Magri D. 1994. Late-quaternary changes of plant biomass as recorded by pollen-stratigraphical data: a discussion of the problem at Valle di Castiglione, Italy. *Review of Palaeobotany and Palynology* **81**: 313–325.

Magri D, Parra I. 2002. Late Quaternary western Mediterranean pollen records and African winds. *Earth and Planetary Science Letters* **200**: 401–408.

Marcott SA, Clark PU, Padman L et al. 2011. Ice-shelf collapse from subsurface warming as a trigger for Heinrich events. *Proceedings of the National Academy of Sciences* **108**: 13415–13419.

Marcott SA, Bauska TK, Buizert C et al. 2014. Centennial-scale changes in the global carbon cycle during the last deglaciation. *Nature* **514**: 616–619.

Margari V, Tzedakis PC, Shackleton NJ et al. 2007. Vegetation response in SW Iberia to abrupt climate change during MIS 6: Direct land-sea comparisons. *Quaternary International* **167–168**: 267–268.

Margari V, Skinner LC, Tzedakis PC et al. 2010. The nature of millennial-scale climate variability during the past two glacial periods. *Nature Geoscience* **3**: 127–131.

Margari V, Skinner LC, Hodell DA et al. 2014. Land-ocean changes on orbital and millennial time scales and the penultimate glaciation. *Geology* **42**: 183–186.

Margari V 2016. Pollen Preparation Protocol for Marine Fossil Pollen. [Online]. Available from: http://www.geog.ucl.ac.uk/about-the-department/supportservices/laboratory/laboratory-methods/lake-sediment-analysis/pollen-preparation-protocol-for-marine-fossil-pollen [accessed 12 January 2020].

Margari V, Skinner LC, Menviel L et al. 2020. Fast and slow components of interstadial warming in the North Atlantic during the last glacial. *Communications Earth & Environment* **1**: 1–9.

Marsicek J, Shuman B, Bartlein PJ et al. 2018. Reconciling divergent trends and millennial variations in Holocene temperatures. *Nature* **554**: 92–96.

Martrat B, Grimalt JO, Shackleton NJ et al. 2007. Four climate cycles of recurring deep and surface water destabilizations on the Iberian margin. *Science* **317**: 502–507.

Martrat B, Jimenez-Amat R, Zahn R et al. 2014. Similarities and dissimilarities between the last two deglaciations and interglaciations in the North Atlantic region. *Quaternary Science Reviews* **99**: 122–134.

Matthews J. 1969. The assessment of a method for the determination of absolute pollen frequencies. *New Phytologist* **68**: 161–166.

McManus JF, Oppo DW, Cullen JL. 1999. A 0.5-Million-Year Record of Millennial-Scale Climate Variability in the North Atlantic. *Science* **283**: 971–975.

Menviel L, Timmermann A, Elison Timm O et al. 2011. Deconstructing the Last Glacial termination: the role of millennial and orbital-scale forcings. *Quaternary Science Reviews* **30**: 1155–1172.

Menviel L, Timmermann A, Friedrich T et al. 2014. Hindcasting the continuum of Dansgaard–Oeschger variability: mechanisms, patterns and timing. *Climate of the Past* **10**: 63–77.

Menviel L, Capron E, Govin A et al. 2019. The penultimate deglaciation: protocol for Paleoclimate Modelling Intercomparison Project (PMIP) phase 4 transient numerical simulations between 140 and 127 ka, version 1.0. *Geoscientific Model Development* **12**: 3649–3685.

Monnin E, Indermühle A, Dällenbach A et al. 2001. Atmospheric CO2 Concentrations over the Last Glacial Termination. *Science* **291**: 112–114.

Monnin E, Steig EJ, Siegenthaler U et al. 2004. Evidence for substantial accumulation rate variability in Antarctica during the Holocene, through synchronization of CO2 in the Taylor Dome, Dome C and DML ice cores. *Earth and Planetary Science Letters* **224**: 45–54.

Morales-Molino C, Devaux L, Georget M et al. 2020. Modern pollen representation of the vegetation of the Tagus Basin (central Iberian Peninsula). *Review of Palaeobotany and Palynology* **276**: 1–15.

Mott RJ, Grant DR, Stea R et al. 1986. Late-glacial climatic oscillation in Atlantic Canada equivalent to the Allerød/Younger Dryas event. *Nature* **323**: 247–250.

Muschitiello F, D'Andrea WJ, Schmittner A et al. 2019. Deep-water circulation changes lead North Atlantic climate during deglaciation. *Nature communications* **10**: 1–10.

Muschitiello F, O'Regan M, Martens J et al. 2020. A new 30 000-year chronology for rapidly deposited sediments on the Lomonosov Ridge using bulk radiocarbon dating and probabilistic stratigraphic alignment. *Geochronology* **2**: 81–91.

Naughton F, Goñi MS, Desprat S et al. 2007. Present-day and past (last 25000 years) marine pollen signal off western Iberia. *Marine Micropaleontology* **62**: 91–114.

Naughton F, Sánchez Goñi MF, Kageyama M et al. 2009. Wet to dry climatic trend in north-western Iberia within Heinrich events. *Earth & Planetary Science Letters* **284**: 329–342.

NGRIP MembersAndersen KK, Azuma N, Barnola JM et al. 2004. High-resolution of Northern Hemisphere climate extending into the last interglacial period. *Nature* **431**: 147–151.

Oliveira D, Desprat S, Yin Q et al. 2018. Unraveling the forcings controlling the vegetation and climate of the best orbital analogues for the present interglacial in SW Europe. *Climate Dynamics* **51**: 667–686.

Pailler D, Bard E. 2002. High frequency palaeoceanographic changes during the past 140 000 yr recorded by the organic matter in sediments of the Iberian Margin. *Palaeogeography, Palaeoclimatology, Palaeoecology* **181**: 431–452.

Pérez FF, Castro CG, Álvarez-Salgado XA et al. 2001. Coupling between the Iberian basin — scale circulation and the Portugal boundary current system: a chemical study. *Deep Sea Research Part I: Oceanographic Research Papers* **48**: 1519–1533.

Pollard D, Barron EJ. 2003. Causes of model–data discrepancies in European climate during oxygen isotope stage 3 with insights from the last glacial maximum. *Quaternary Research* **59**: 108–113.

Polley HW, Johnson HB, Marinot BD et al. 1993. Increase in C3 plant water-use efficiency and biomass over Glacial to present CO2 concentrations. *Nature* **361**: 61–64.

Polunin O, Smithies BE. 1973. *Flowers of South-West Europe*. Oxford University Press: London.

Rasmussen SO, Andersen KK, Svensson A et al. 2006. A new Greenland ice core chronology for the last glacial termination. *Journal of Geophysical Research* **111**: 1–16.

Rasmussen SO, Bigler M, Blockley SP. et al. 2014. A stratigraphic framework for abrupt climatic changes during the Last Glacial period based on three synchronized Greenland ice-core records: refining and extending the INTIMATE event stratigraphy. *Quaternary Science Reviews* **106**: 14–28.

Reille M. 1999. Pollen et spores d'Europe et d'Afrique du Nord. Laboratoire de Botanique Historique et Palynologie: Marseille.

Reimer PJ, Brown TA, Reimer RW. 2004. Discussion: Reporting and Calibration of Post-Bomb 14C Data. *Radiocarbon* **46**: 1299–1304.

Reimer PJ, Austin WEN, Bard E et al. 2020. The INTCAL20 Northern Hemisphere radiocarbon age calibration curve (0–55 CAL kBP) Part of: IntCal 20. *Radiocarbon* **62**: 1–33.

Relvas P, Barton ED, Dubert J et al. 2007. Physical oceanography of the western Iberia ecosystem: Latest views and challenges. *Progress in Oceanography* **74**: 149–173.

Renssen H, Goosse H, Fichefet T et al. 2001. The 8.2 ka BP event simulated by a Global Atmosphere—Sea-Ice—Ocean Model. *Global Planetary Science Letters* **28**: 1567–1570.

Rodrigues T, Grimalt JO, Abrantes F et al. 2010. The last glacial–interglacial transition (LGIT) in the western mid-latitudes of the North Atlantic: Abrupt sea surface temperature change and sea level implications. *Quaternary Science Reviews* **29**: 1853–1862.

Rodríguez S, Querol X, Alastuey A et al. 2001. Saharan dust contributions to PM10 and TSP levels in Southern and Eastern Spain. *Atmospheric Environment* **35**: 2433–2447.

Salgueiro E, Naughton F, Voelker AHL et al. 2014. Past circulation along the western Iberian margin: a time slice vision from the Last Glacial to the Holocene. *Quaternary Science Reviews* **106**: 316–329.

Sánchez Goñi MFS, Eynaud F, Turon JL et al. 1999. High resolution palynological record off the Iberian margin: direct land-sea correlation for the Last Interglacial complex. *Earth and Planetary Science Letters* **171**: 123–137.

Sánchez Goñi MFS, Turon JL, Eynaud F et al. 2000. European Climatic Response to Millennial-Scale Changes in the Atmosphere–Ocean System during the Last Glacial Period. *Quaternary Research* **54**: 394–403.

Sessford EG, Jensen MF, Tisserand AA et al. 2019. Consistent fluctuations in intermediate water temperature off the coast of Greenland and Norway during Dansgaard-Oeschger events. *Quaternary Science Reviews* **223**: 1–16.

Shackleton NJ, Hall MA, Vincent E. 2000. Phase relationships between millennial-scale events 64,000–24,000 years ago. *Paleoceanography* **15**: 565–569.

Shackleton NJ, Sánchez Goñi MF, Pailler D et al. 2003. Marine Isotope Substage 5e and the Eemian Interglacia. *Global and Planetary Change* **36**: 151–155.

Skinner LC, Muschitiello F, Scrivner AE. 2019. Marine reservoir age variability over the last deglaciation: implications for marine CarbonCycling and prospects for regional radiocarbon calibrations. *Paleoceanography and Paleoclimatology* **34**: 1807–1815.

Skinner LC, Shackleton NJ, Elderfield H. 2003. Millennial-scale variability of deep-water temperature and δ18Odw indicating deep-water source variations in the Northeast Atlantic, 0–34 cal. ka BP. *Geochemistry, Geophysics, Geosystems* **4**: 1–17.

Skinner LC, Freeman E, Hodell D et al. 2021. Atlantic Ocean Ventilation Changes Across the Last Deglaciation and Their Carbon Cycle Implications. *Paleoceanography and Paleoclimatology* **36**: 1–21.

Stern JV, Lisiecki LE. 2013. North Atlantic circulation and reservoir age changes over the past 41,000 years. *Geophysical Research Letters* **40**: 3693–3697.

Stockhecke M, Timmermann A, Kipfer R et al. 2016. Millennial to orbital-scale variations of drought intensity in the Eastern Mediterranean. *Quaternary Science Reviews* **133**: 77–95.

Stockmarr J. 1971. Tablets with spores used in absolute pollen analysis. *Pollen et Spores* **13**: 615–621.

Stuiver M, Polach HA. 1977. Discussion Reporting of 14C Data. *Radiocarbon* **19**: 355–363.

Synal H-A, Stocker M, Suter M. 2007. MICADAS: A new compact radiocarbon AMS system. *Nuclear Instruments and Methods in Physics Research Section B: Beam Interactions with Materials and Atoms* **259**: 7–13.

Thomas ER, Wolff EW, Mulvaney R et al. 2007. The 8.2 ka event from Greenland ice cores. *Quaternary Science Reviews* **26**: 70–81.

Tinner W, Lotter AF. 2001. Central European vegetation response to abrupt climate change at 8.2 ka. *Geology* 29: 551–554.

Turon JL, Lézine AM, Denèfle M. 2003. Land–sea correlations for the last glaciation inferred from a pollen and dinocyst record from the portuguese margin. *Quaternary Research* 59: 88–96.

Tzedakis PC, Roucoux KH, de Abreu L *et al.* 2004. The Duration of Forest Stages in Southern Europe and Interglacial Climate Variability. *Geology* 306: 2231–2235.

Tzedakis PC. 2010. The MIS 11 – MIS 1 analogy, southern European vegetation, atmospheric methane and the "early anthropogenic hypothesis". *Climate of the Past* 6: 131–144.

Tzedakis PC, Drysdale RN, Margari V *et al.* 2018. Enhanced climate instability in the North Atlantic and southern Europe during the Last Interglacial. Nature. *Communications* 9: 1–14.

Vale C. 1990. Temporal variations of particulate metals in the Tagus River Estuary. *Science of the Total Environment* 97–98: 137–154.

Vale C, Sundby B. 1987. Suspended sediment fluctuations in the Tagus estuary on semi-diurnal and fortnightly time scales. *Estuarine, Coastal and Shelf Science* 25: 495–508.

Vale C, Cortesão C, Castro O *et al.* 1993. Suspended-sediment response to pulses in river flow and semidiurnal and fortnightly tidal variations in a mesotidal estuary. *Marine Chemistry* 43: 21–31.

van Aken HM. 2000a. The hydrography of the mid-latitude Northeast Atlantic Ocean: II: The intermediate water masses. *Deep Sea Research Part I: Oceanographic Research Papers* 47: 789–824.

van Aken HM. 2000b. The hydrography of the mid-latitude northeast Atlantic Ocean: I: The deep water masses. *Deep Sea Research Part I: Oceanographic Research Papers* 47: 757–788.

van der Knaap WO, van Leeuwen JFN. 1995. Holocene vegetation succession and degradation as responses to climatic change and human activity in the Serra de Estrela. *Portugal. Review of Palaeobotany & Palynology* 89: 153–211.

van der Knaap WO, van Leeuwen JFN. 1997. Late Glacial and early Holocene vegetation succession, altitudinal vegetation zonation, and climatic change in the Serra da Estrela, Portugal. *Review of Palaeobotany & Palynology* 97: 239–285.

Vanney JR, Mougenot D. 1981. La plate-forme continentale du Portugal et les provinces adjacentes: analyse géomorphologique. Serviços Geológicos de Portugal: Lisbon.

Vautravers MJ, Shackleton NJ. 2006. Centennial-scale surface hydrology off Portugal during marine isotope stage 3: Insights from planktonic foraminiferal fauna variability. *Paleoclimatology and Paleoceanography* 21: 1–13.

Vis G-J, Kasse C, Vandenberghe J. 2008. Late Pleistocene and Holocene palaeogeography of the Lower Tagus Valley (Portugal): effects of relative sea level, valley morphology and sediment supply. *Quaternary Science Reviews* 27: 1682–1709.

Vis G-J, Kasse C, Kroon D *et al.* 2016. Time-integrated 3D approach of late Quaternary sediment-depocentermigration in the Tagus depositional system: From river valley to abyssal plain. *Earth Science Reviews* 153: 192–211.

Vis G-J, Kasse C. 2009. Late Quaternary valley-fill succession of the Lower Tagus Valley, Portugal. *Sedimentary Geology* 221: 19–39.

Vitorino J, Oliveira A, Jouanneau JM *et al.* 2002. Winter dynamics on the northern Portuguese shelf. Part 1: physical processes. *Progress in Oceanography* 52: 129–153.

Voelker AH, de Abreu L, Schönfeld J *et al.* 2009. Hydrographic conditions along the western Iberian margin during marine isotope stage 2. *Geochemistry, Geophysics, Geosystems* 10: 1–30.

Voelker AH, de Abreu L. 2011. A review of abrupt climate change events in the northeastern Atlantic Ocean (Iberian Margin): Latitudinal, longitudinal, and vertical gradients. In *Abrupt Climate Change: Mechanisms, Patterns, and Impacts*, Rashid H, Polyak L, Mosley-Thompson E (eds). Geophysical Monograph Series: Washington, DC; 15–37.

Von Grafenstein U, Erlenkeuser H, Müller J *et al.* 1998. The cold event 8200 years ago documented in oxygen isotope records of precipitation in Europe and Greenland. *Climate Dynamics* 14: 73–81.

Wacker L, Christl M, Synal HA. 2010. Bats: A new tool for AMS data reduction. *Nuclear Instruments and Methods in Physics Research Section B: Beam Interactions with Materials and Atoms* 269: 976–979.

Wacker L, Lippold J, Molná M *et al.* 2013. Towards radiocarbon dating with single foraminifera with a gas ion source. *Nuclear Instruments and Methods in Physics Research B* 294: 307–310.

Waelbroeck C, Duplessy J-C, Michel E, Labeyrie L, Paillard D, Duprat J. 2001. The timing of the last deglaciation in North Atlantic climate records. *Nature* 412: 724–727.

Waelbroeck C, Labeyrie L, Michel E *et al.* 2002. Sea-level and deep water temperature changes derived from benthic foraminifera isotopic records. *Quaternary Science Reviews* 21: 295–305.

Watts WA. 1977. The Late Devensian vegetation of Ireland. *Philosophical Transactions of the Royal Society of London B* 280: 273–293.

Watts WA. 1980. Regional variation in the response of vegetation to Lateglacial climatic events in Europe. In *In Studies in the Late Glacial of North–West Europe*, Lowe J, Gray J, Robinson JE (eds). Pergamon Press: Oxford; 1–21.

West G, Kaufman DS, Muschitiello F *et al.* 2019. Amino acid racemization in Quaternary foraminifera from the Yermak Plateau, Arctic Ocean. *Geochronology* 1: 53–67.

Williams JW, Blois JL, Shuman BN. 2011. Extrinsic and intrinsic forcing of abrupt ecological change: case studies from the late Quaternary. *Journal of Ecology* 99: 664–677.

Wolf D, Kolb T, Alcaraz-Castaño M *et al.* 2018. Climate deteriorations and Neanderthal demise in interior Iberia. *Scientific Reports* 8: 1–10.

Wolf D, Ryborz K, Kolb T *et al.* 2019. Origins and genesis of loess deposits in central Spain, as indicated by heavy mineral compositions and grain-size variability. *Sedimentology* 66: 1139–1161.

Yokoyama Y, Lambeck K, De Deckker P *et al.* 2000. Timing of the Last Glacial Maximum from observed sea-level minima. *Nature* 405: 713–716.